Control of Flare-Induced Shock Wave - Boundary Layer Interaction using Micro Vortex Generators

T. Nilavarasan

Department of Aerospace Engineering

Defence Institute of Advanced Technology

India

Flare induced shock – boundary layer interaction

- Shock – Boundary layer interactions over launch vehicles and missiles
- Structural resonant frequencies of skin panels
- Extremely perilous in low-supersonic/ transonic regimes and when the vehicle experiences high dynamic pressure.
- Inter-stage flares – axisymmetric compression corner-induced interactions

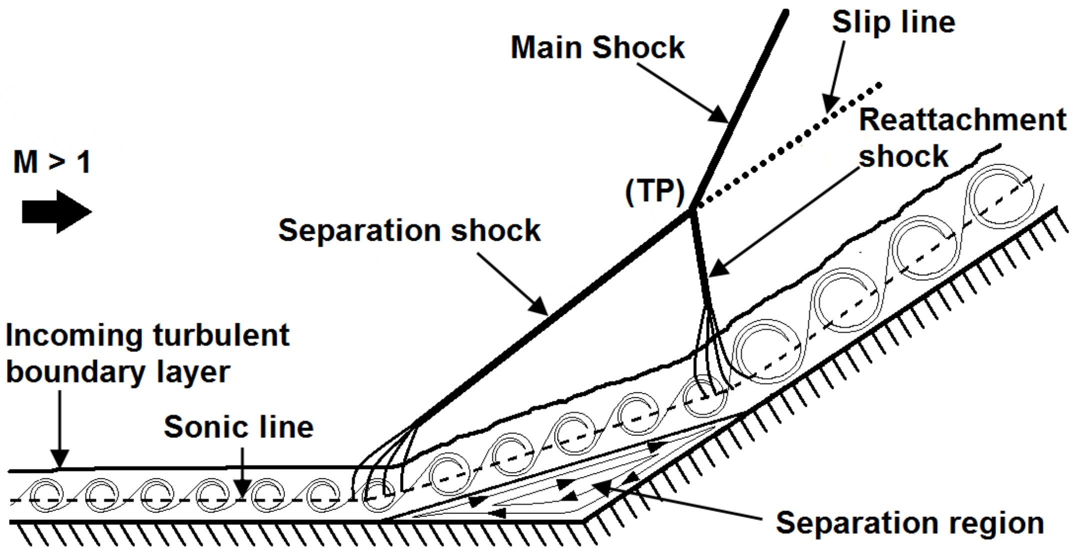

Schematic representation of the Shock - Boundary Layer Interaction around a flare.

Supersonic flow over a flared Axisymmetric Body

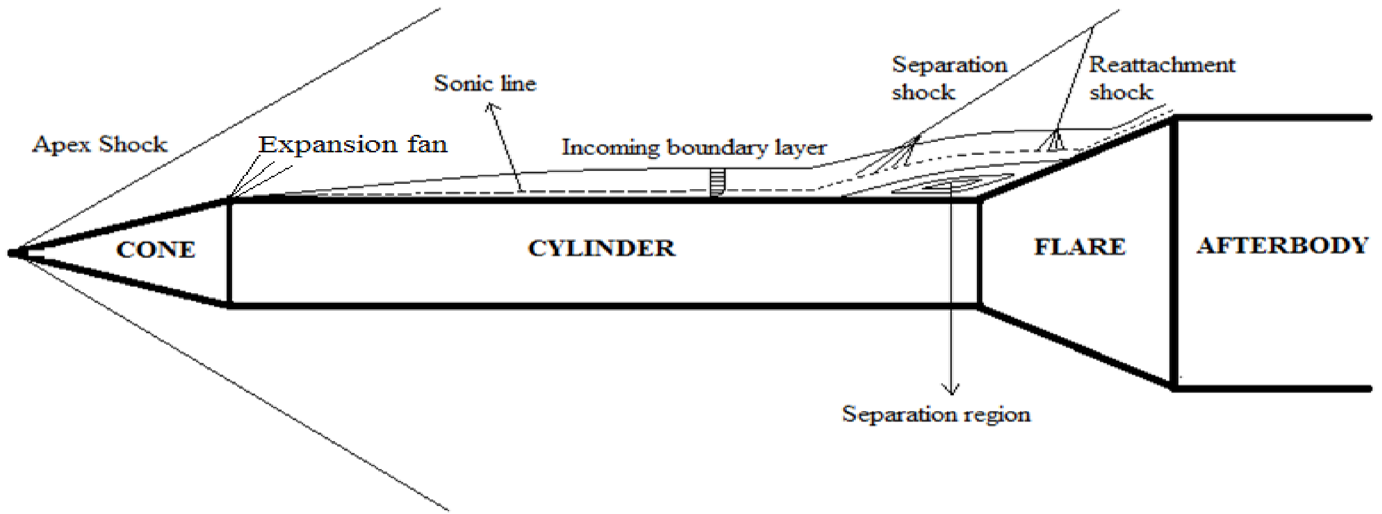

Control of Shock – Boundary Layer Interactions

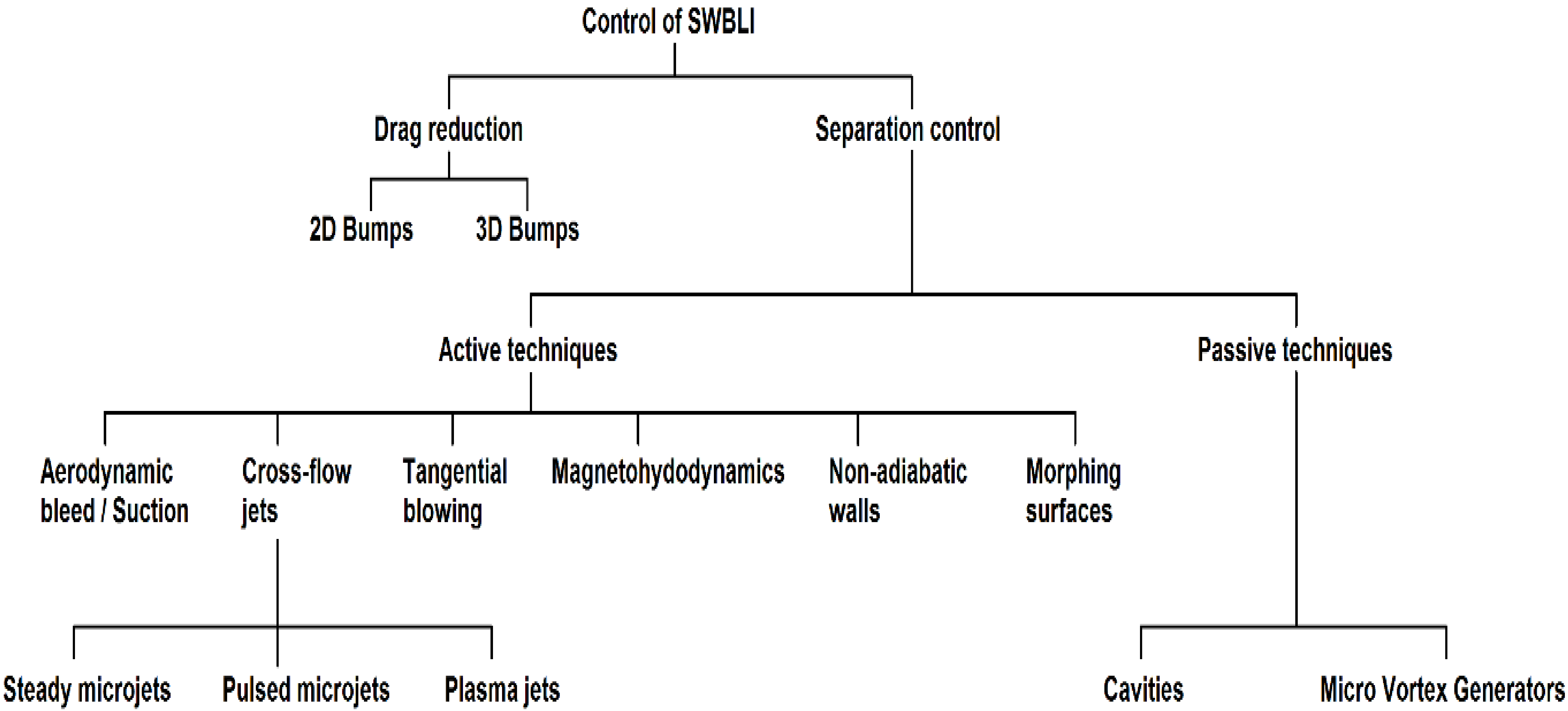

Micro Vortex Generators (MVGs)

1. Widely popular passive control technique – simpler design and no power penalty
2. Sub-boundary layer protuberances capable of producing streamwise vortices
3. Alternate bands of upwash and downwash regions in the incoming boundary layer

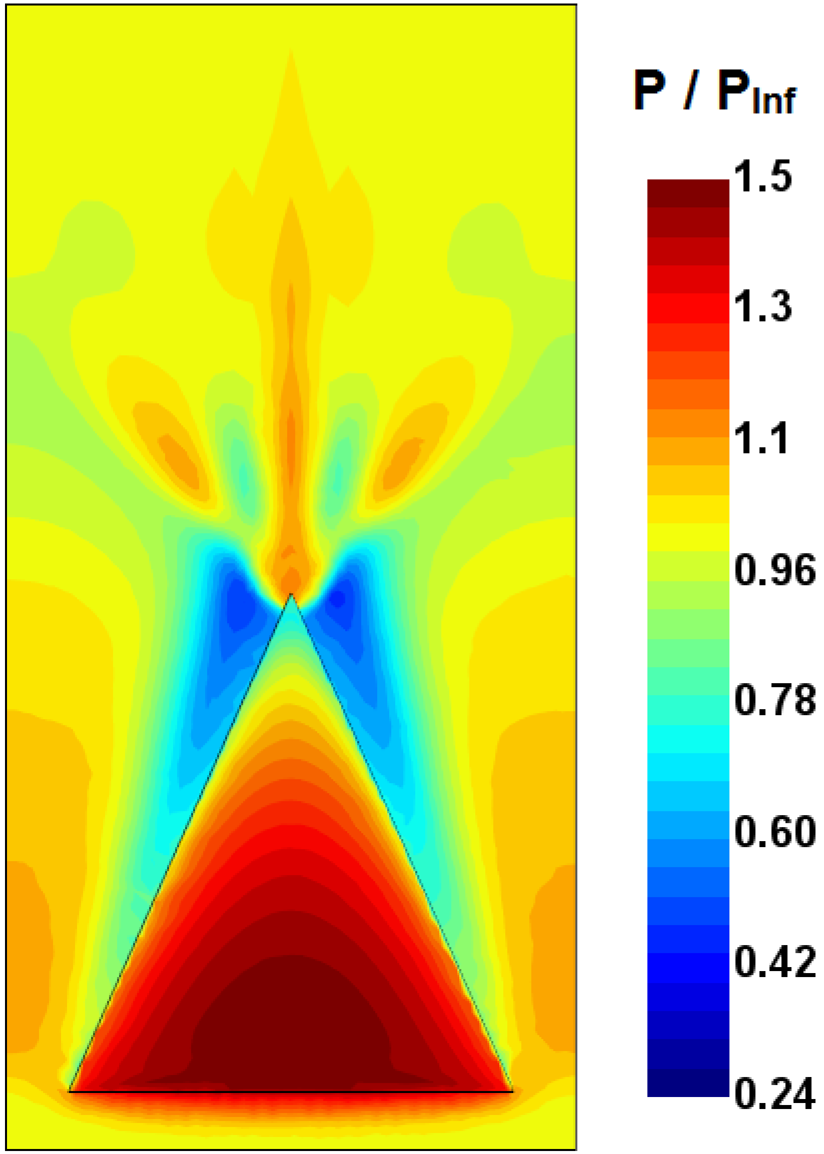

Spanwise pressure difference induced by an MVG

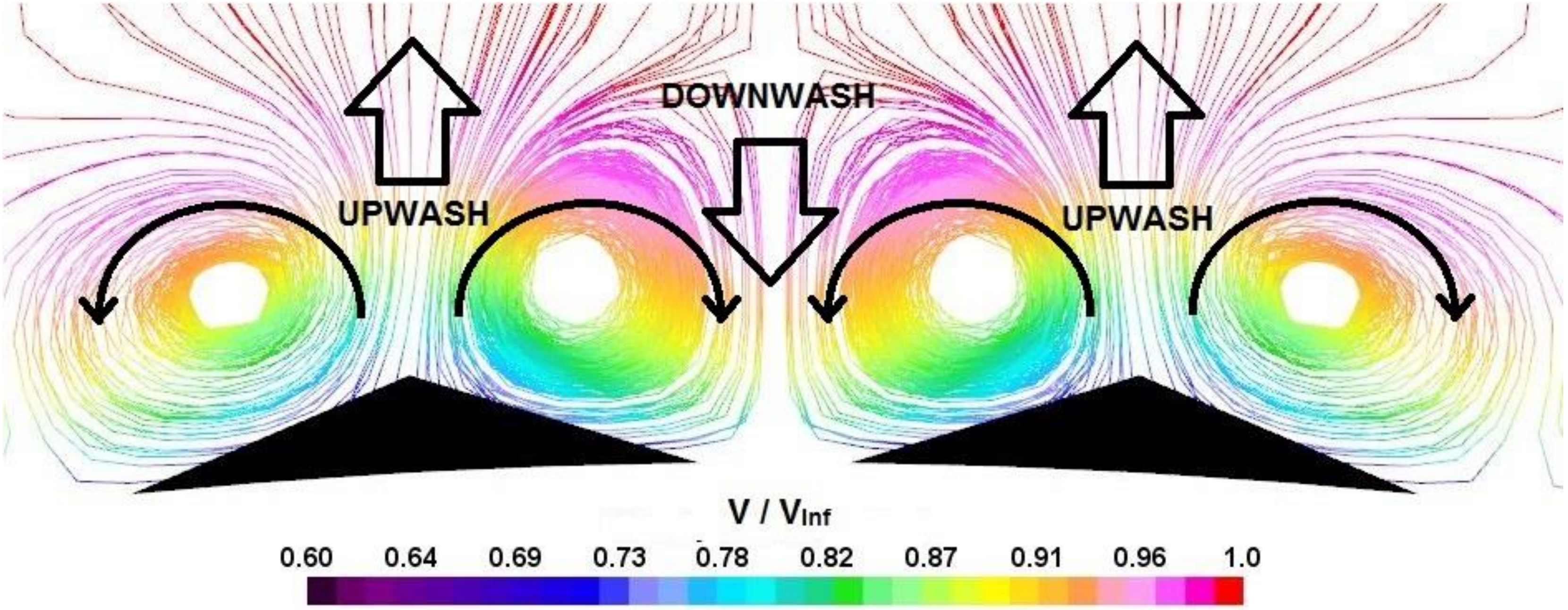

Cross sectional streamlines showing the counter-rotating vortices

Objectives of the study

1. To characterize the low-frequency shock oscillations due to a flare-induced flow separation.

2. To understand the flow physics involved in delaying the onset of shock-induced flow separation near an axisymmetric compression corner using Micro Vortex Generators (MVGs).

3. To investigate the role played by various geometrical parameters of MVGs such as shape, size, trailing edge height and streamwise position on their separation control performance.

4. To bring out the topological modifications induced by MVGs in the separation region.

5. To analyse the alterations caused by the MVGs in the unsteady behaviour of the separation shock.

Wind tunnel model and flow conditions

Test Mach number	2.05 ± 0.02
Free Stream Velocity	523 m/s
Stagnation Pressure	208.5 kPa ± 2%
Stagnation Temperature	298 K ± 0.4%
Unit Reynolds number	25.257 x 10^6 m^{-1}

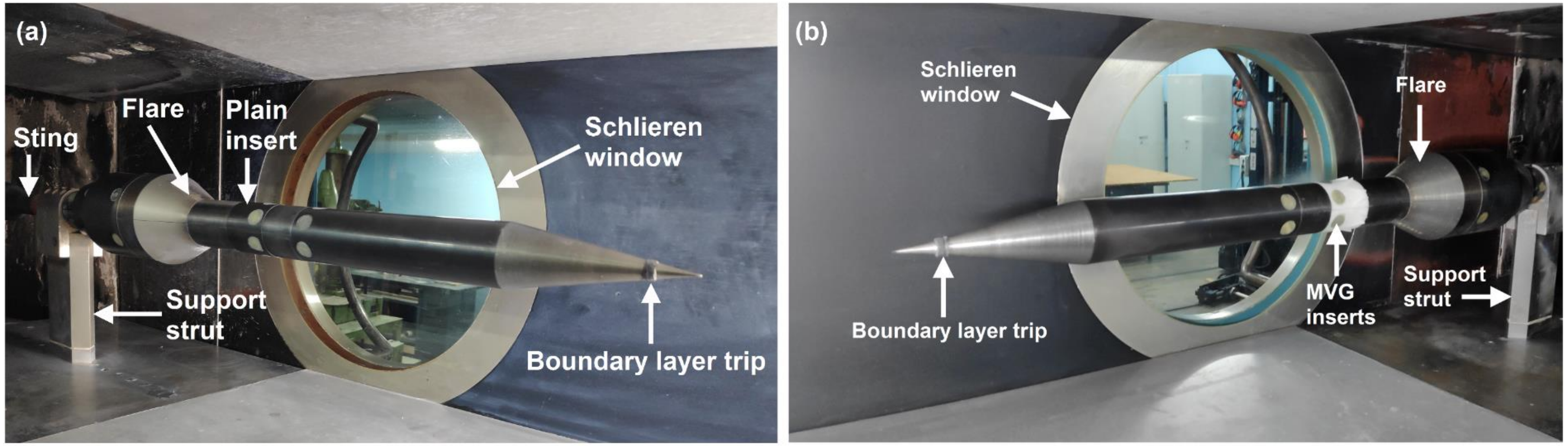

Model mounted inside the wind tunnel (a) baseline; (b) with MVG inserts

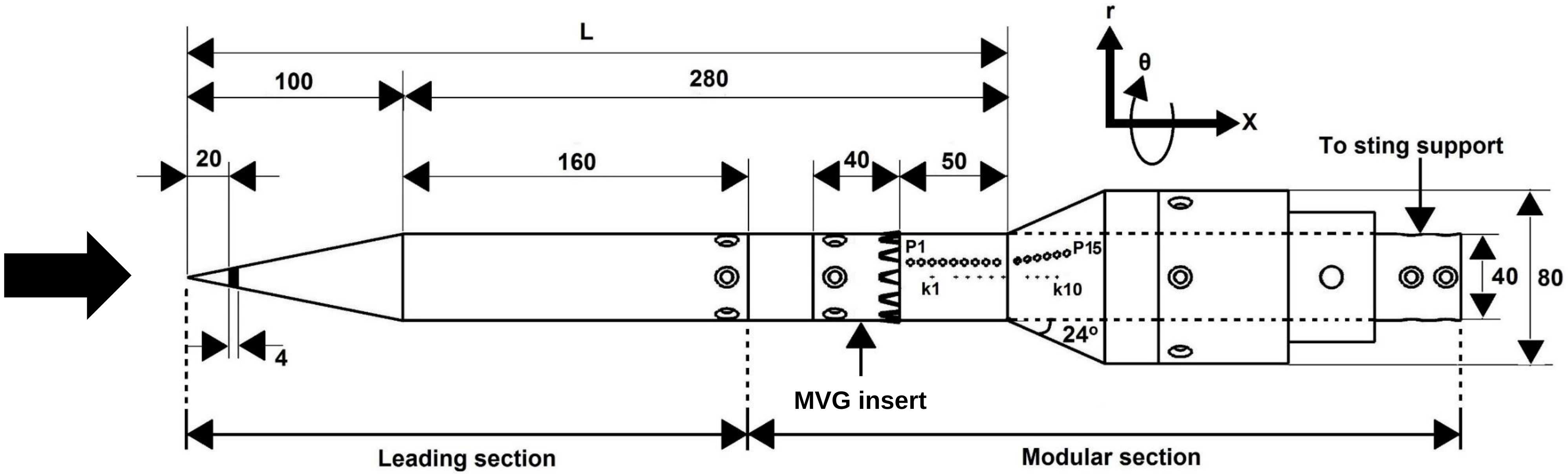

Schematic diagram of test model (All dimensions are in mm)

Pressure measurements

1. 10 Kulite miniature pressure transducers (Model No: XCQ-093)

2. Sampling rate = 50 kHz, with 20 kHz low pass filter.

3. Seven point calibration (with fourth order polynomial fit).

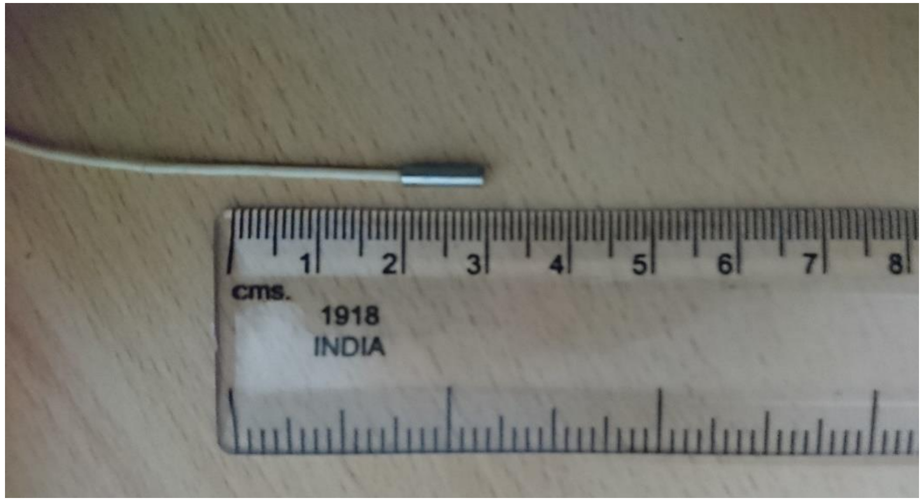

Kulite XCQ - 093

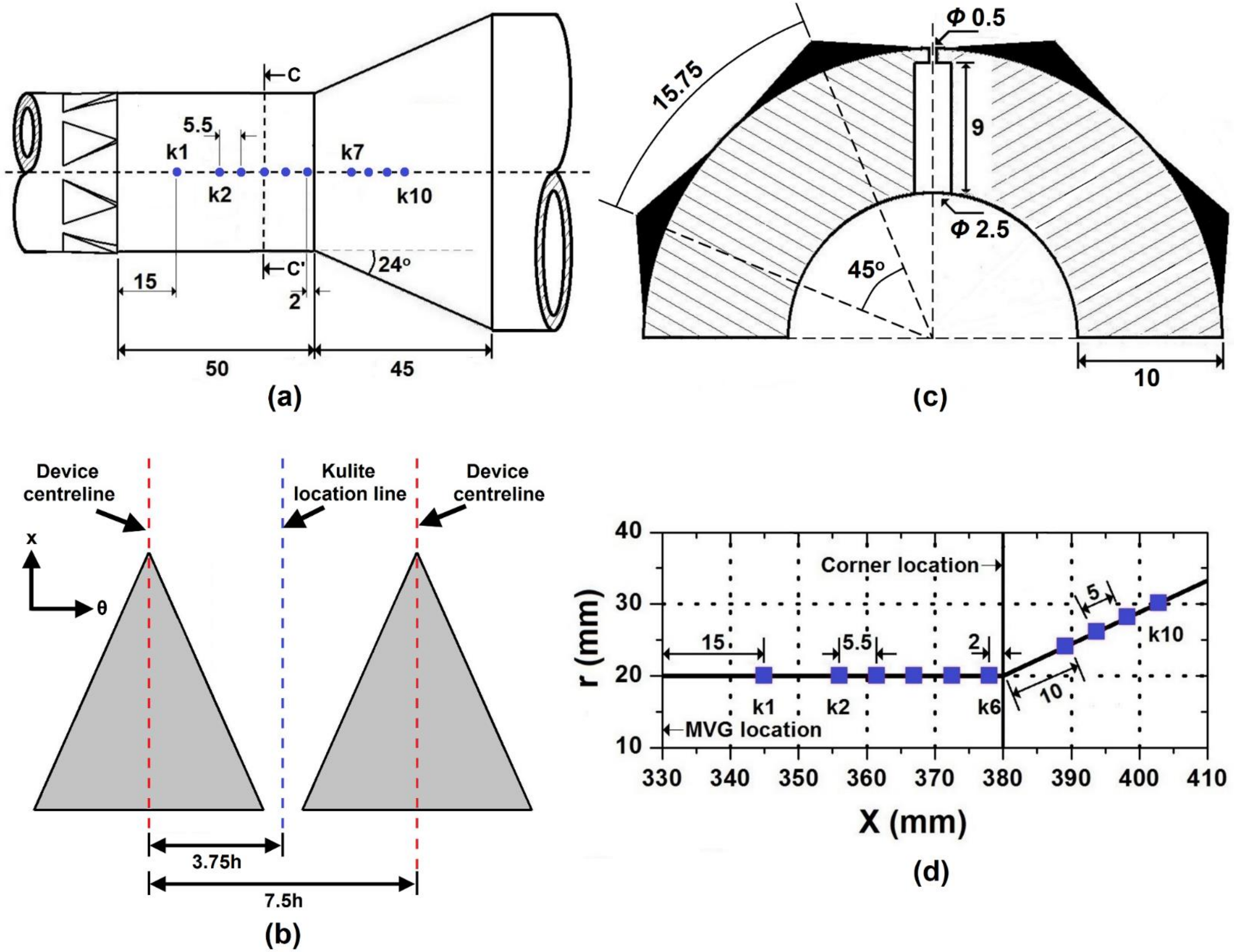

(a) Top view of model near the area of interest; (b) Sectional rear view of the half cylindrical segment from CC'; (c,d) Streamwise location of Kulites and ESP ports.

Flow visualization techniques

Z-Type Schlieren imaging

1. Horizontal knife-edge arrangement
2. Image resolution: 1280 x 780 pixels
3. Pixel density: 3.2 pixels/mm.
4. 60 fps; 50 frames in 0.83 seconds
5. Exposure time: 125 μs

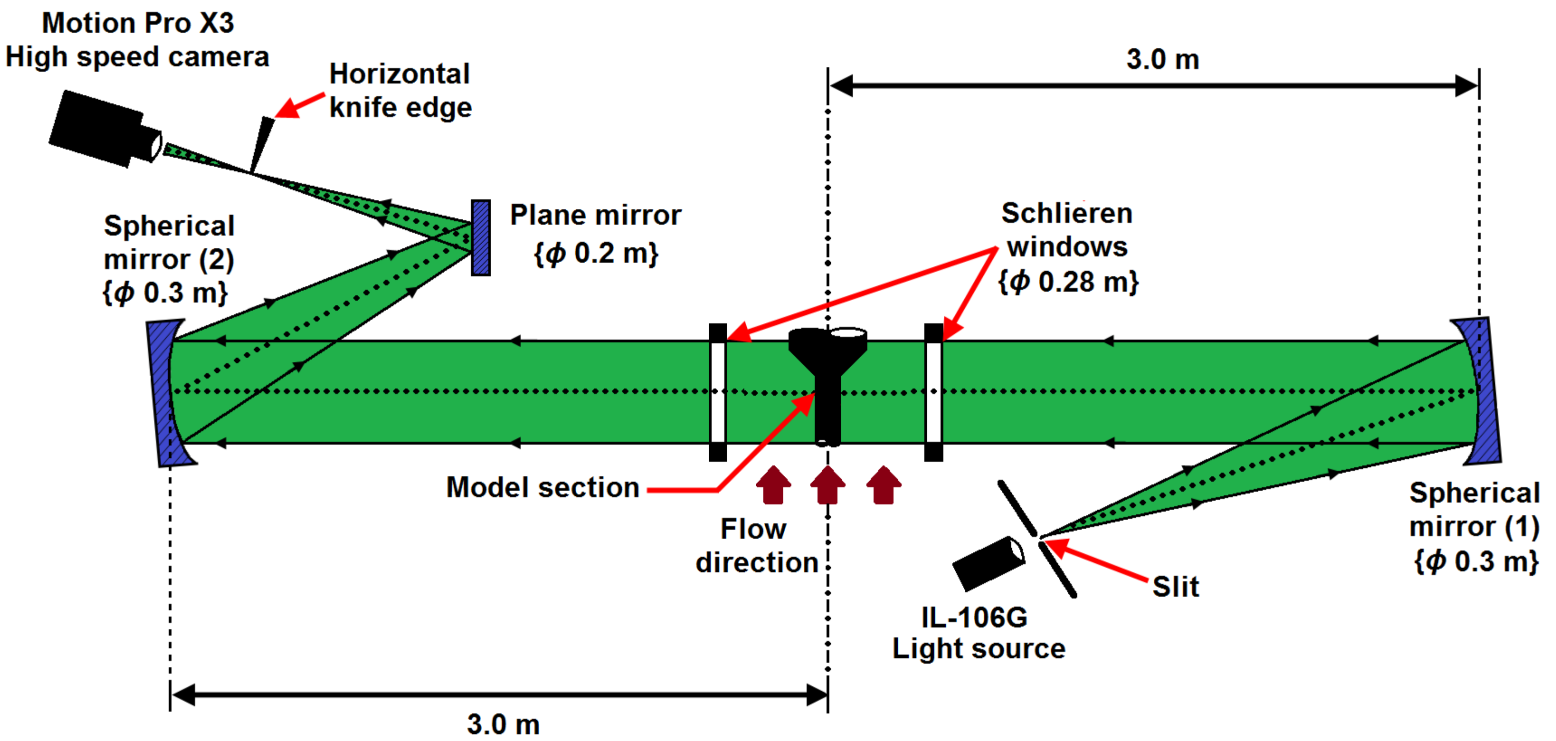

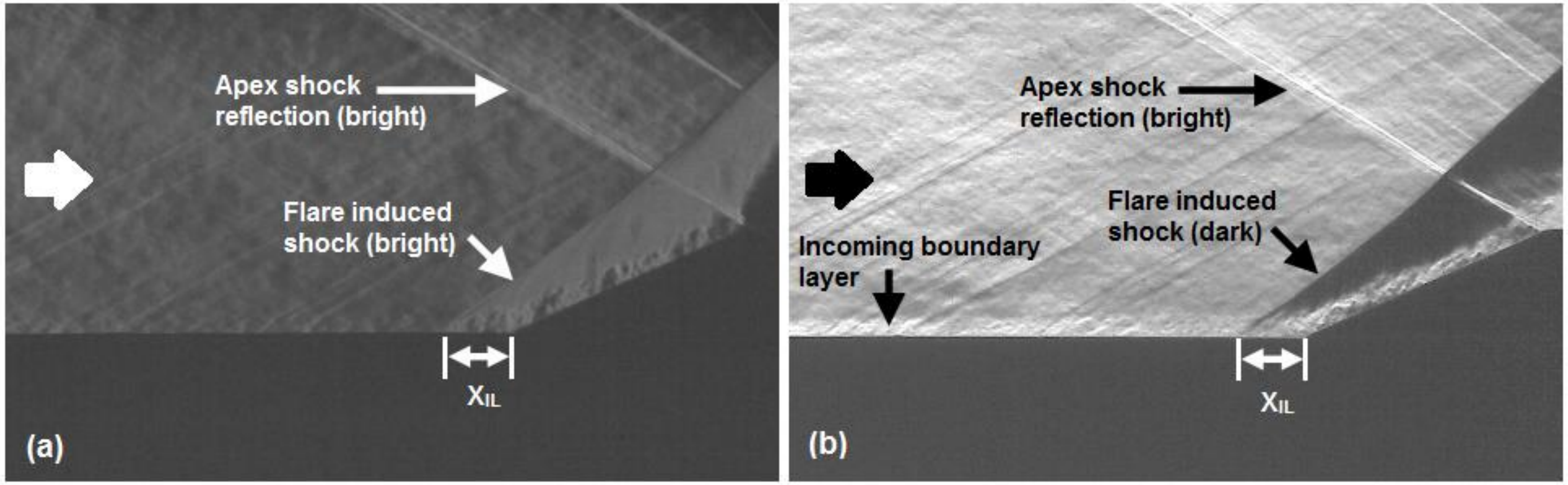

Surface Oil Flow Visualization

1. A mixture of TiO_2, Vacuum pump oil (ISO Grade 32) and Oleic Acid (TiO_2/Oil/Oleic = 10:5:1).
2. 13 seconds blowdown time

Computational setup and flow domain

SOLVER SETUP

- STAR CCM+
- Solver – Density Based, Steady-Implicit
- Turbulence model – Spalart-Allmaras model
- Advection Upwind Splitting Method (AUSM)
- Discretization – Second Order Upwind Scheme
- Fluid medium – Air (Ideal gas)
- Viscosity – Sutherland law

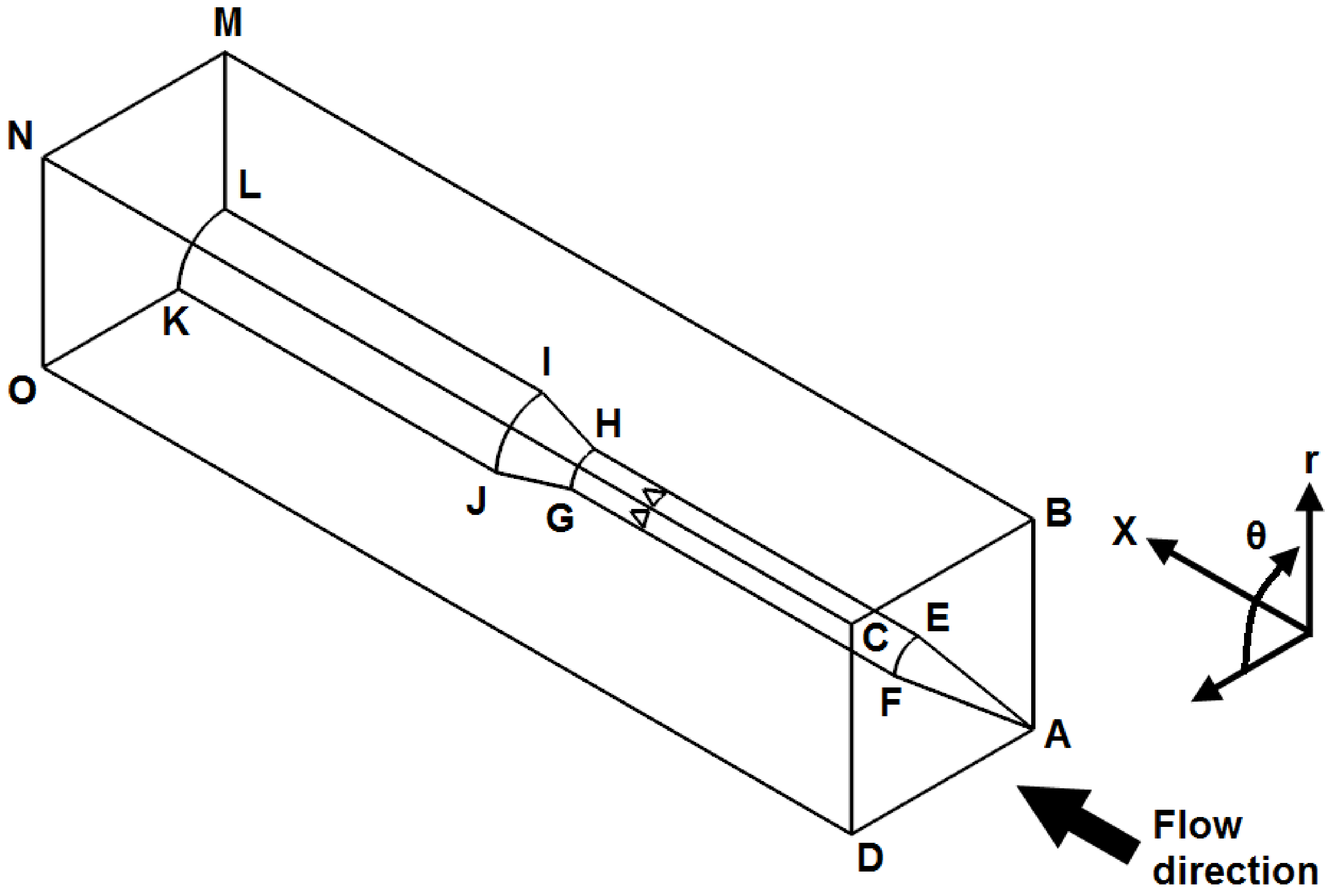

Computational domain

Meshing strategy

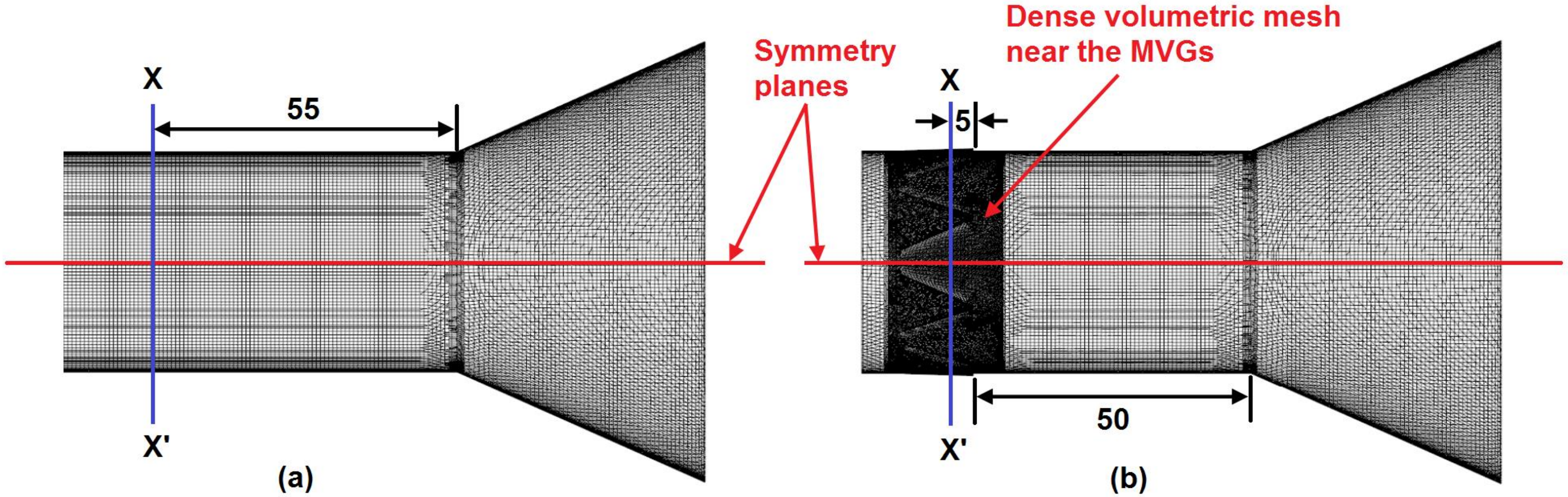

Surface mesh (a) Uncontrolled; (b) Controlled (BR).

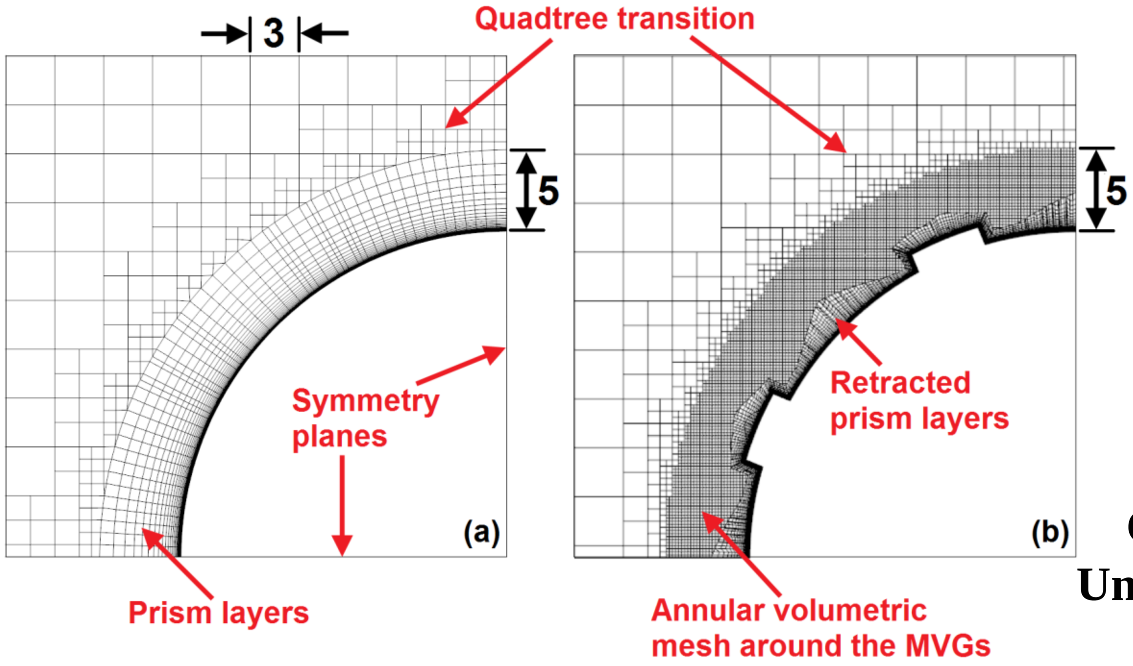

Cross-section at XX' (a) Uncontrolled; (b) Controlled (BR).

- Predominantly hexahedral grid
- Interior base cell size = 3 mm
- Dense surface mesh (Max. cell size = 0.75 mm)
- 50 prismatic layers within 5 mm (Growth rate = 1.2)
- Very dense annular volumetric mesh around the MVGs (Max. cell size = 0.3 mm
- Prism layers retracted over the MVG surfaces

Code validation for Flare induced Shock – Boundary Layer interaction

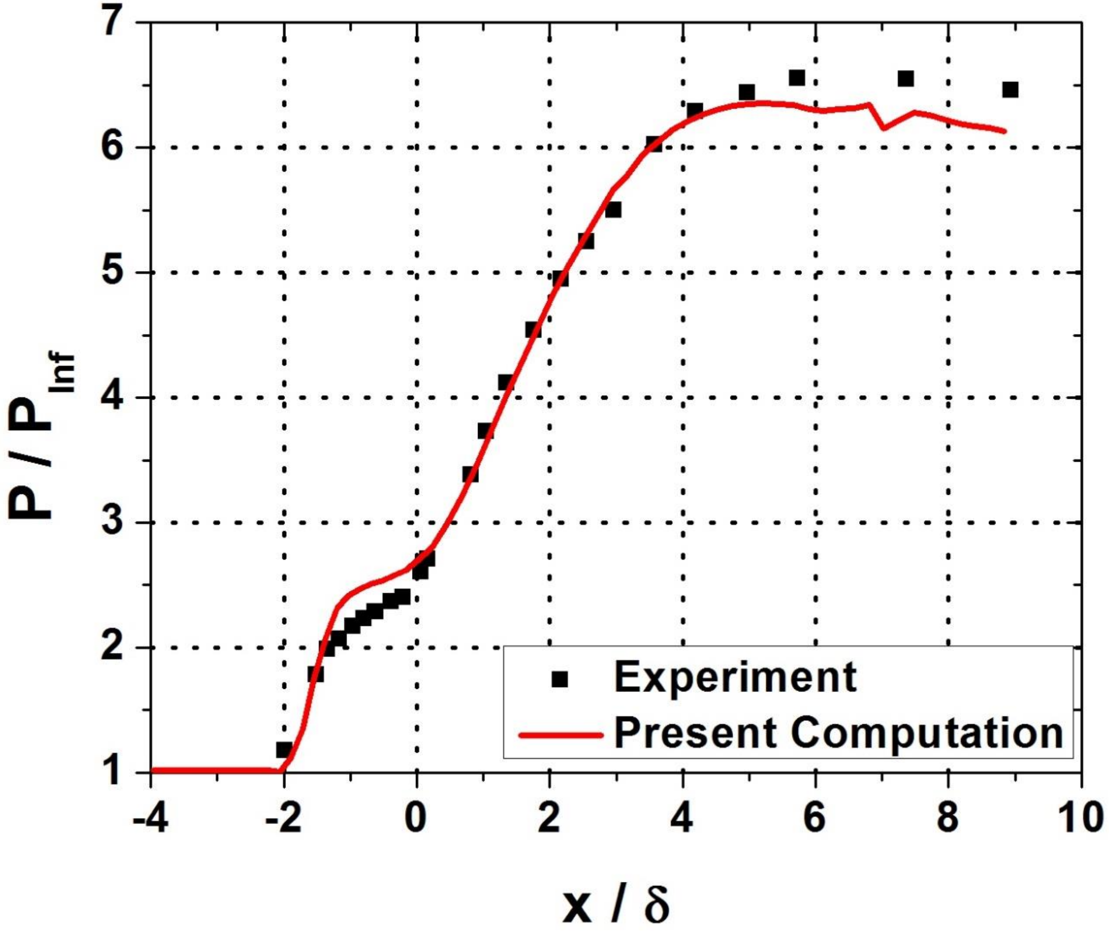

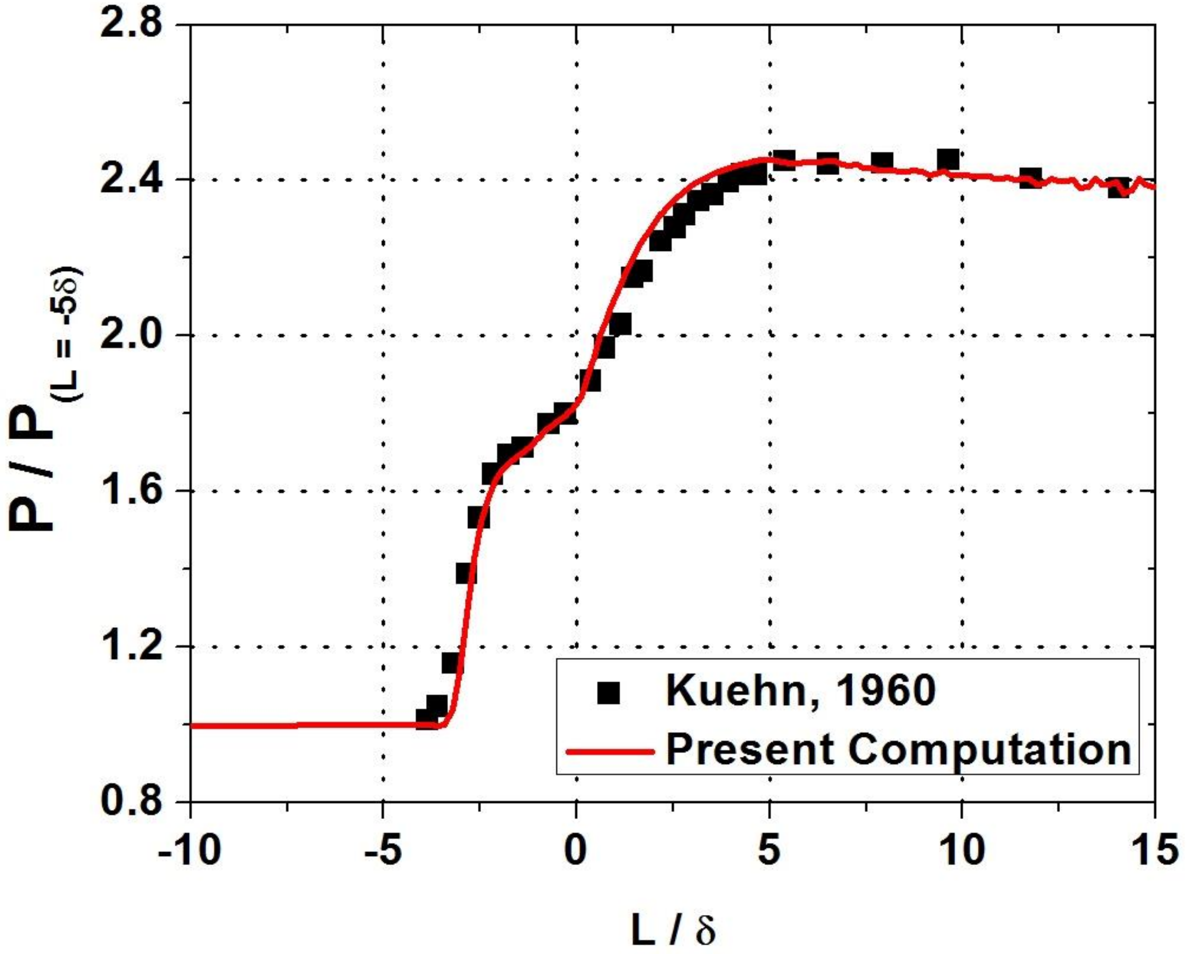

- Hollow Cylinder-Flare model (Roshko and Thomke, 1976)
- Mach number = 3.96
- Flare angle = 25°
- Boundary layer thickness, δ = 10.4 mm

- Cone-Cylinder-Flare model (Kuehn, 1960)
- Mach number = 1.97
- Flare angle = 25°
- Boundary layer thickness, δ = 4 mm

Code validation – In the vicinity of MVGs (PSP from Herges et al, 2010)

Ability of the computational code to predict intricate flowfield characteristics in the vicinity of the MVGs was shown by numerical simulating the experiments performed by **Herges et.al (2010)** and comparing the PSP data with the present numerical data.

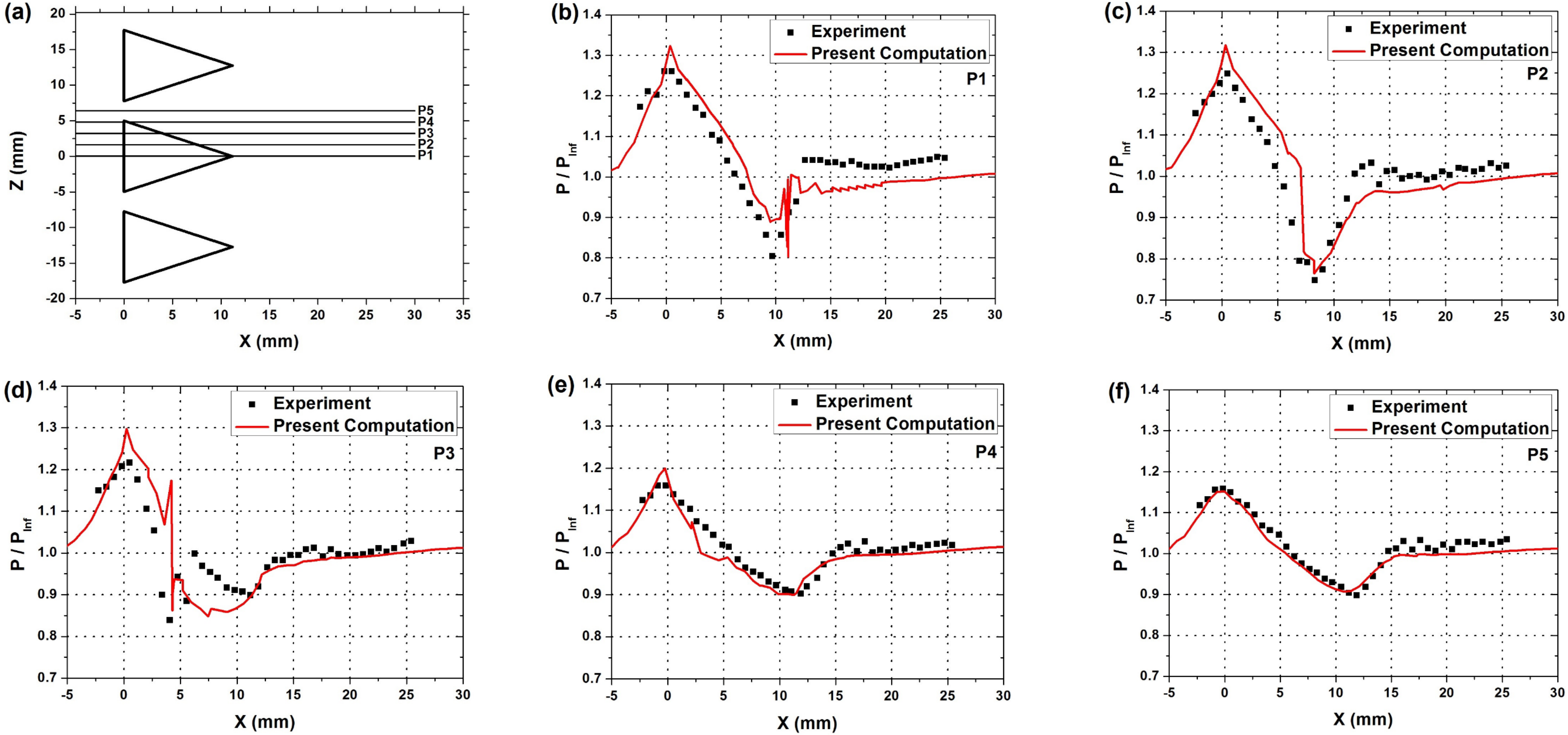

Uncontrolled interaction

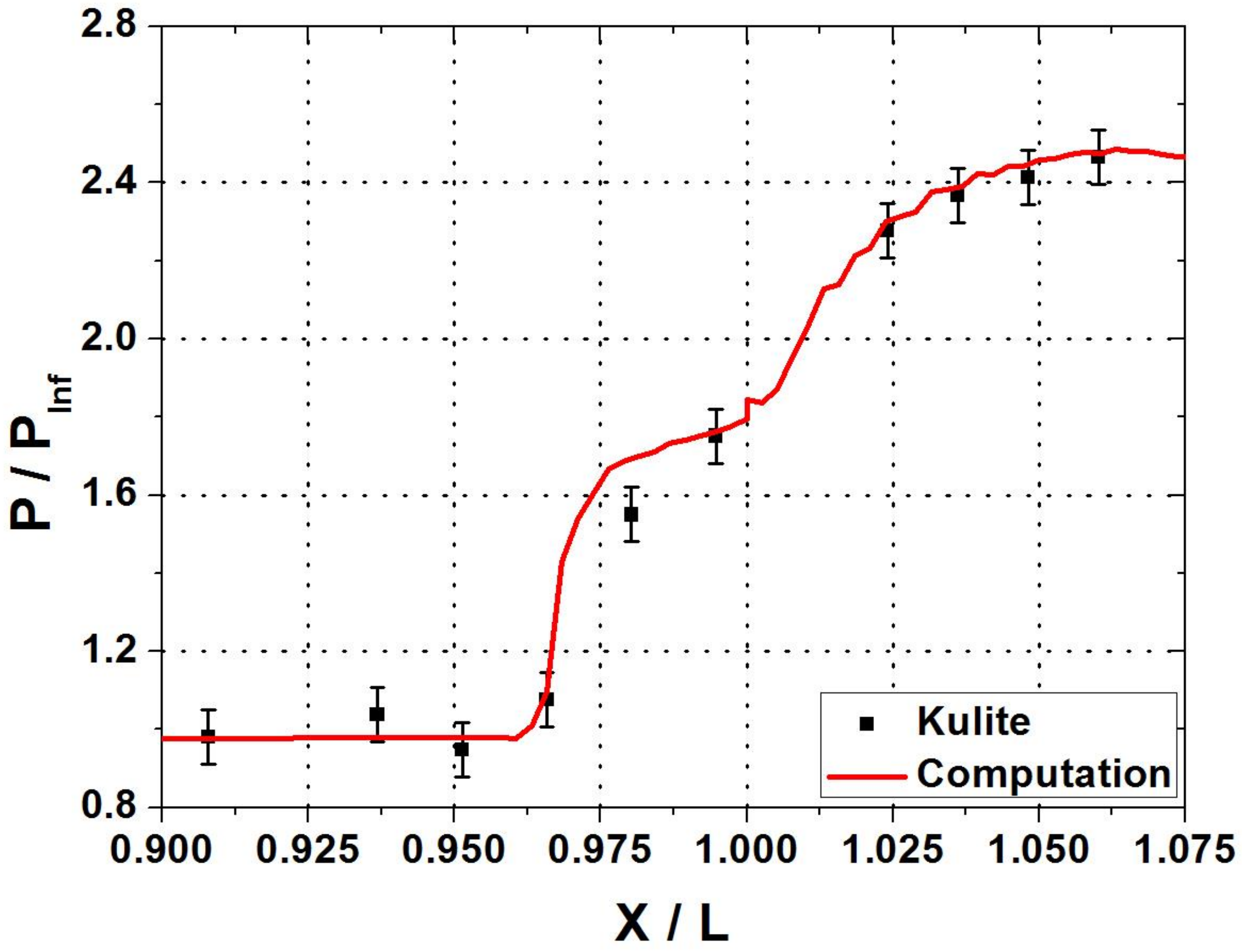

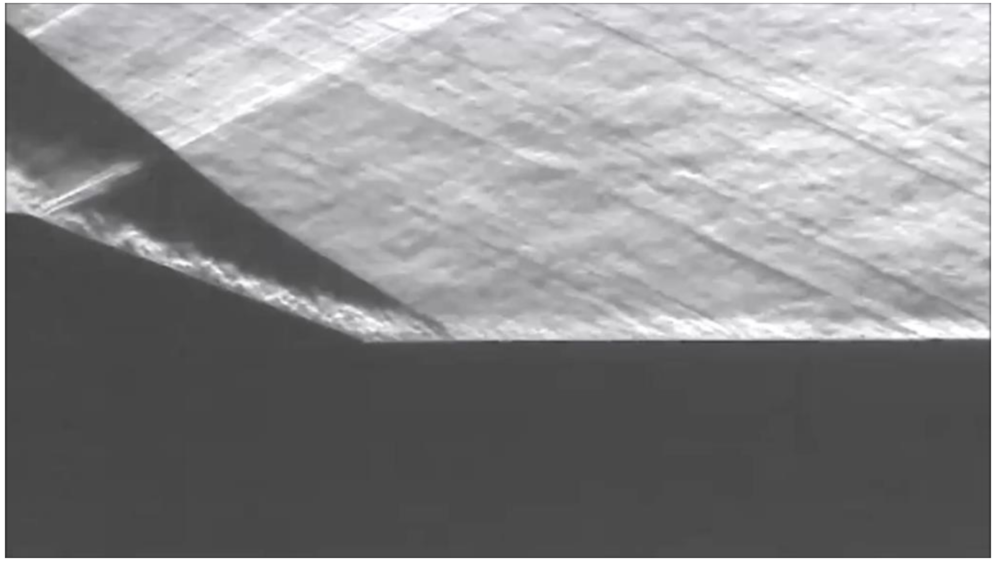

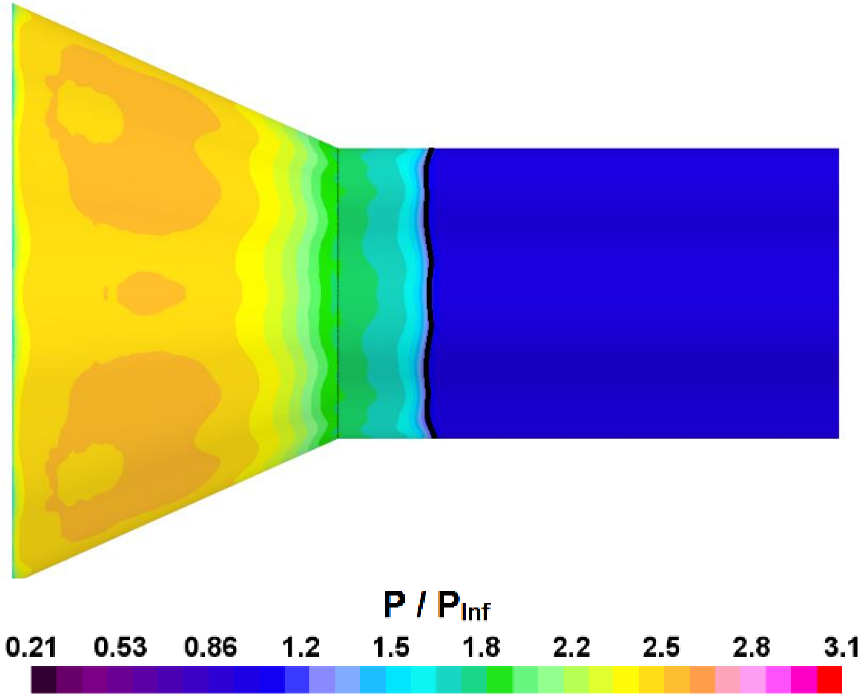

Uncontrolled interactions

Separation length, $X_{S(U)}$ = 12 mm

Reattachment wavelength, λ = 15 mm

Radius of curvature, R_C = 56.76 mm

Goertler number, G = 2.16×10^4

Threshold Goertler number, G_T = 2.66×10^3

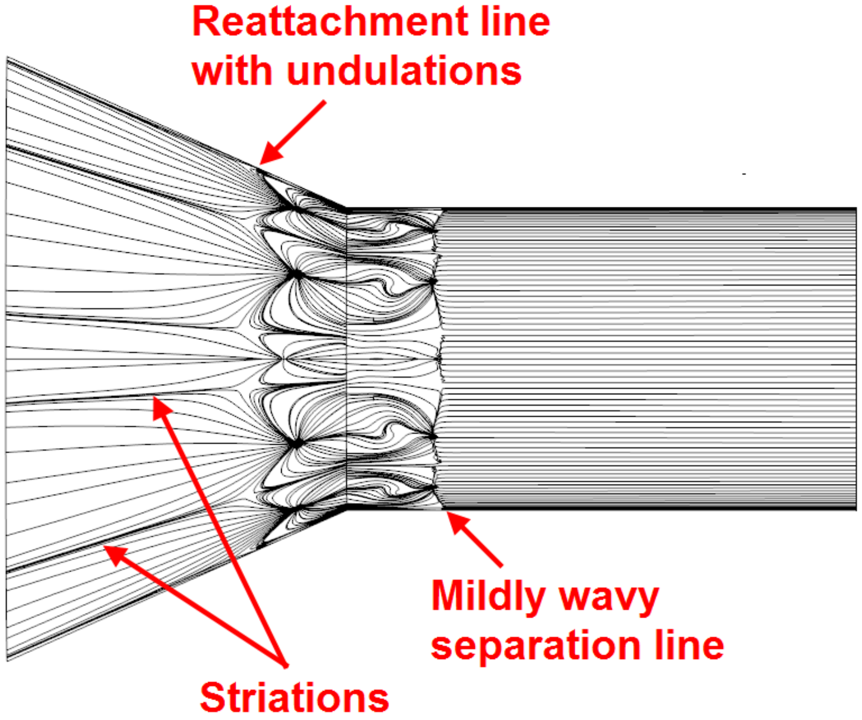

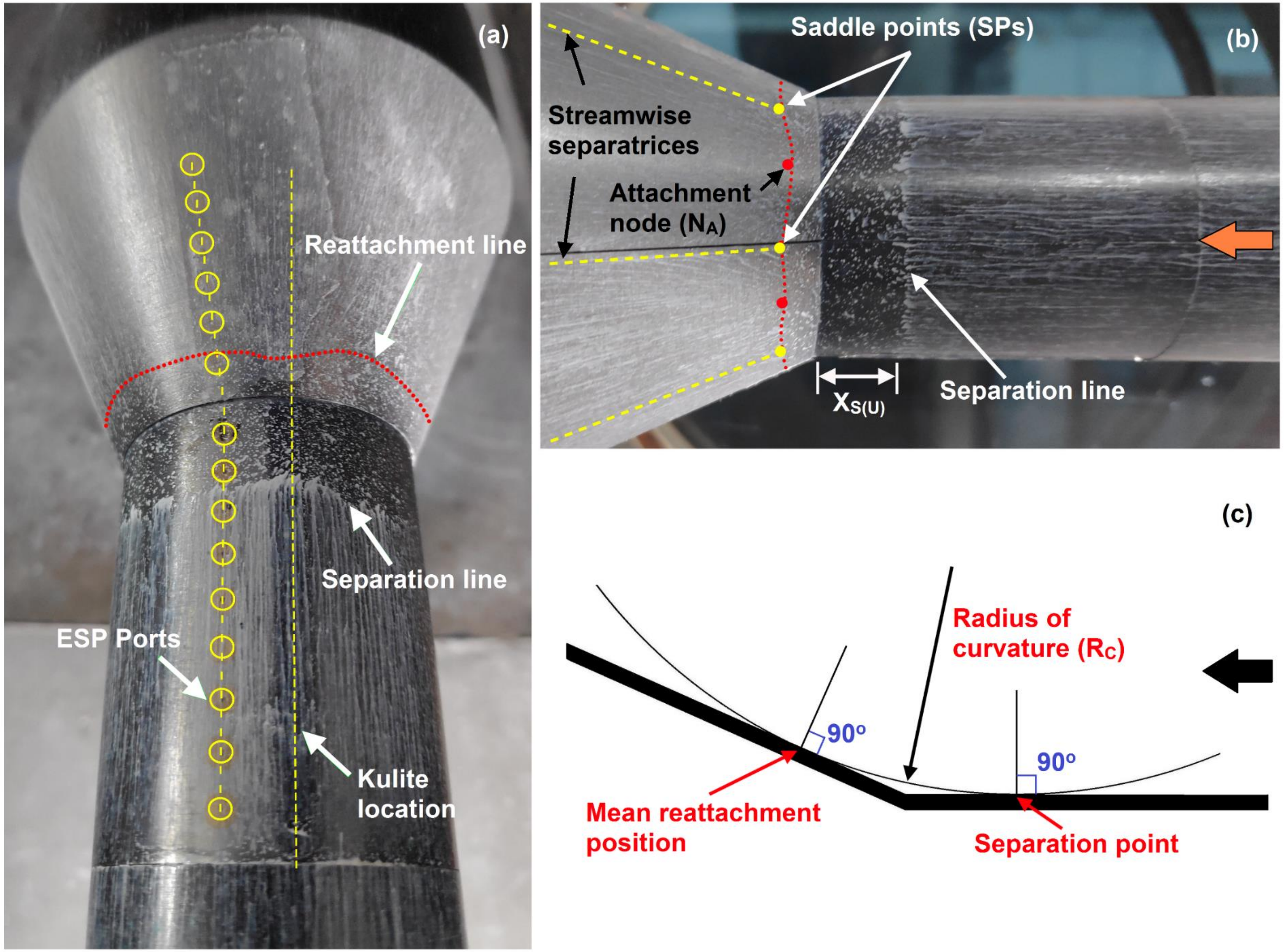

(a) Top view (b) Side view and (c) Schematic diagram of the flow topology

Performance evaluation of different MVG shapes

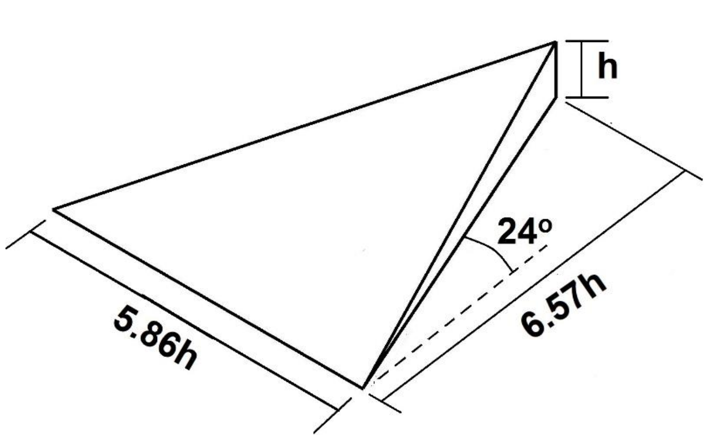

Baseline Ramp (BR)

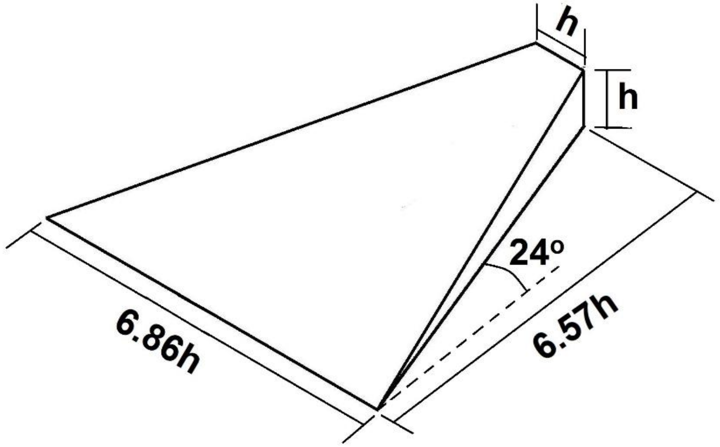

Trapezoidal Ramp (TZ)

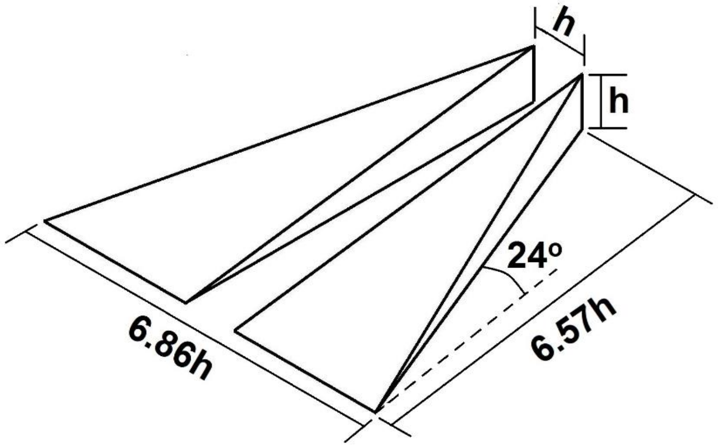

Split Ramp (SR)

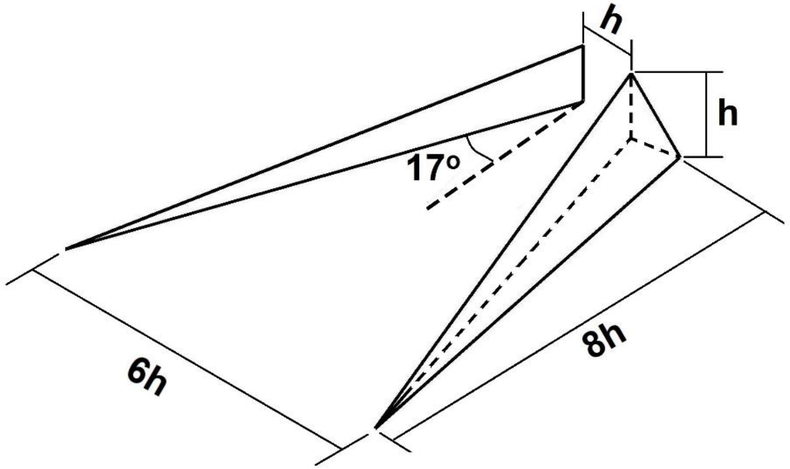

Thick Vanes (TV)

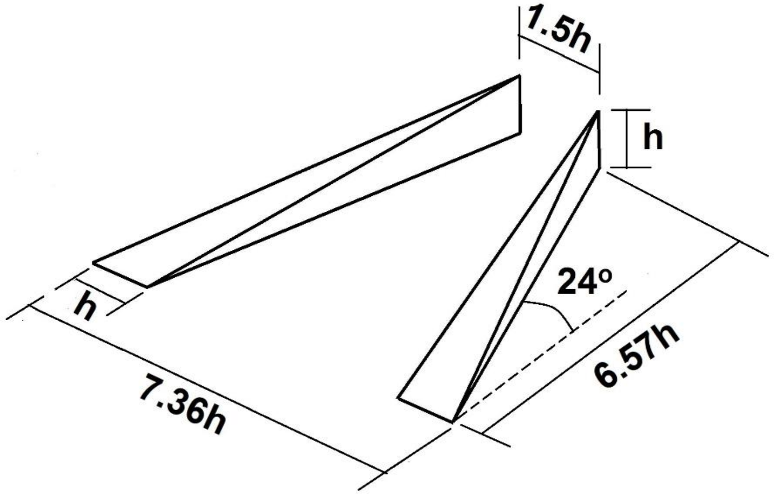

Ramped Vanes (RV)

MVG size and arrangement

$$\pi d = n \, x \, 7.5h$$

n	h (mm)
4	4.2
5	3.4
6	**2.8**
7	2.4
8	**2.1**
9	1.9
10	1.7
11	1.5
12	**1.4**
13	1.3
14	1.2
15	1.1

- Diameter, d = 40 mm
- Local boundary layer thickness at 50 mm upstream of the corner = 4.2 mm (δ_{MVG})
- Device height, h = 1.4 mm (0.33 δ_{MVG})

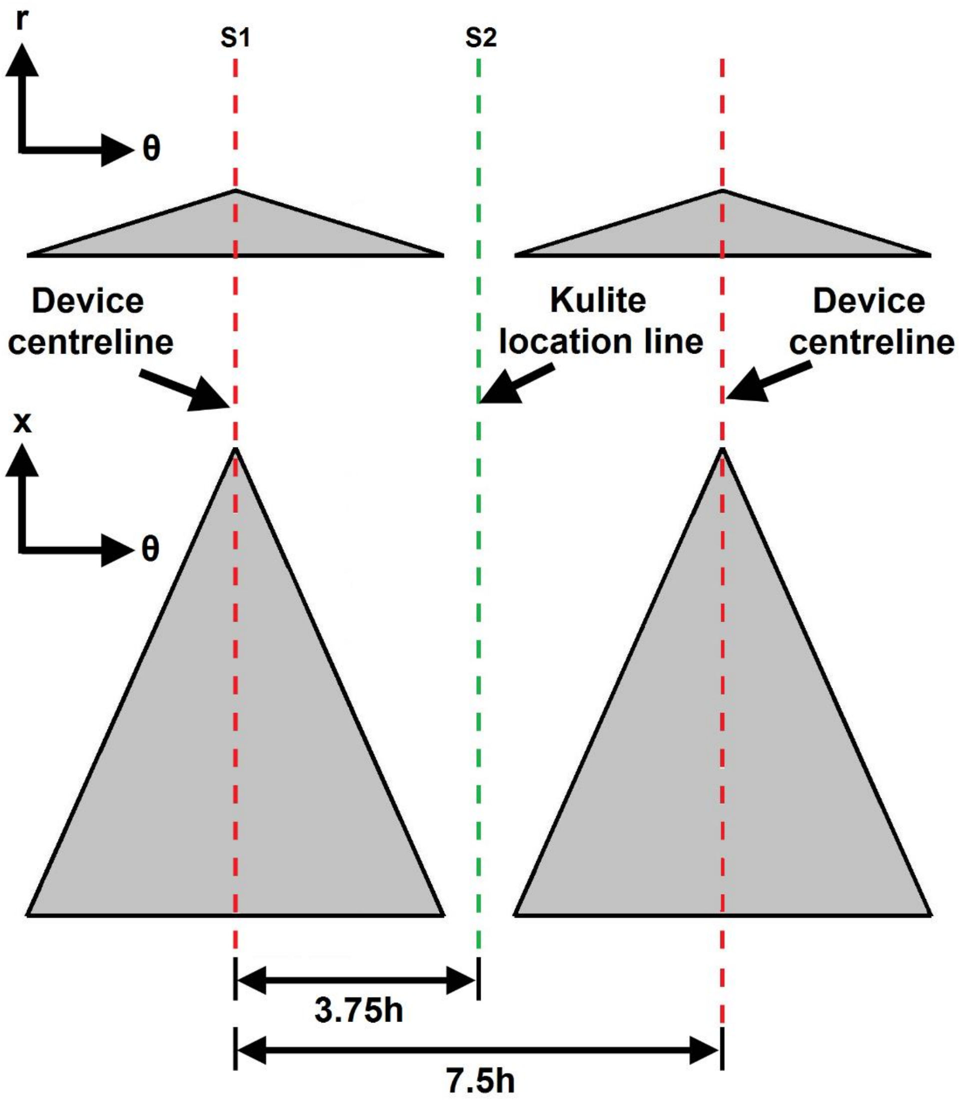

CFD Validation with present experimental data

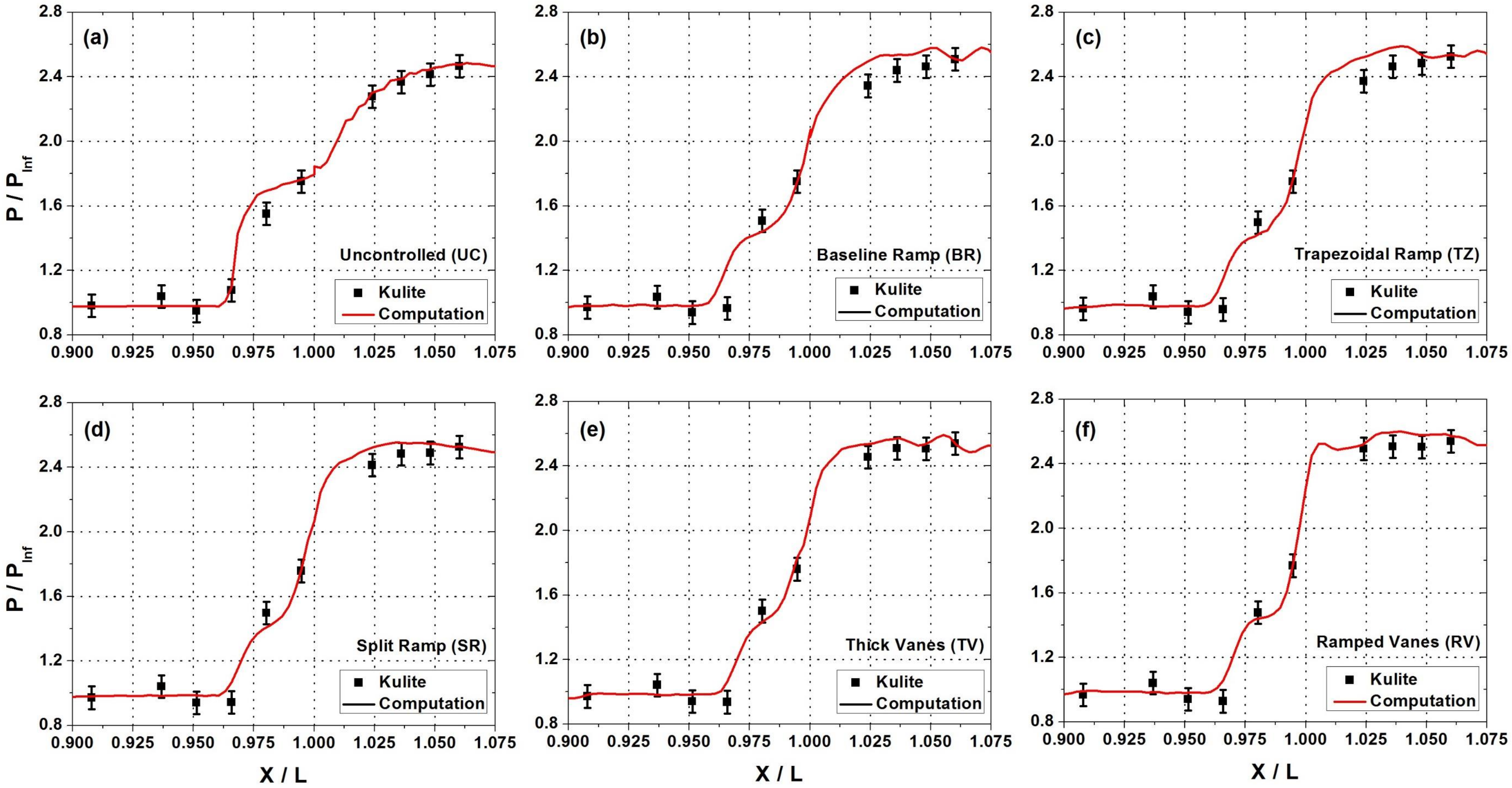

Time-averaged Schlieren photographs

(a) Uncontrolled

(b) Baseline Ramp

(c) Trapezoidal Ramp

(d) Split Ramp

(e) Thick Vanes

(f) Ramped Vanes

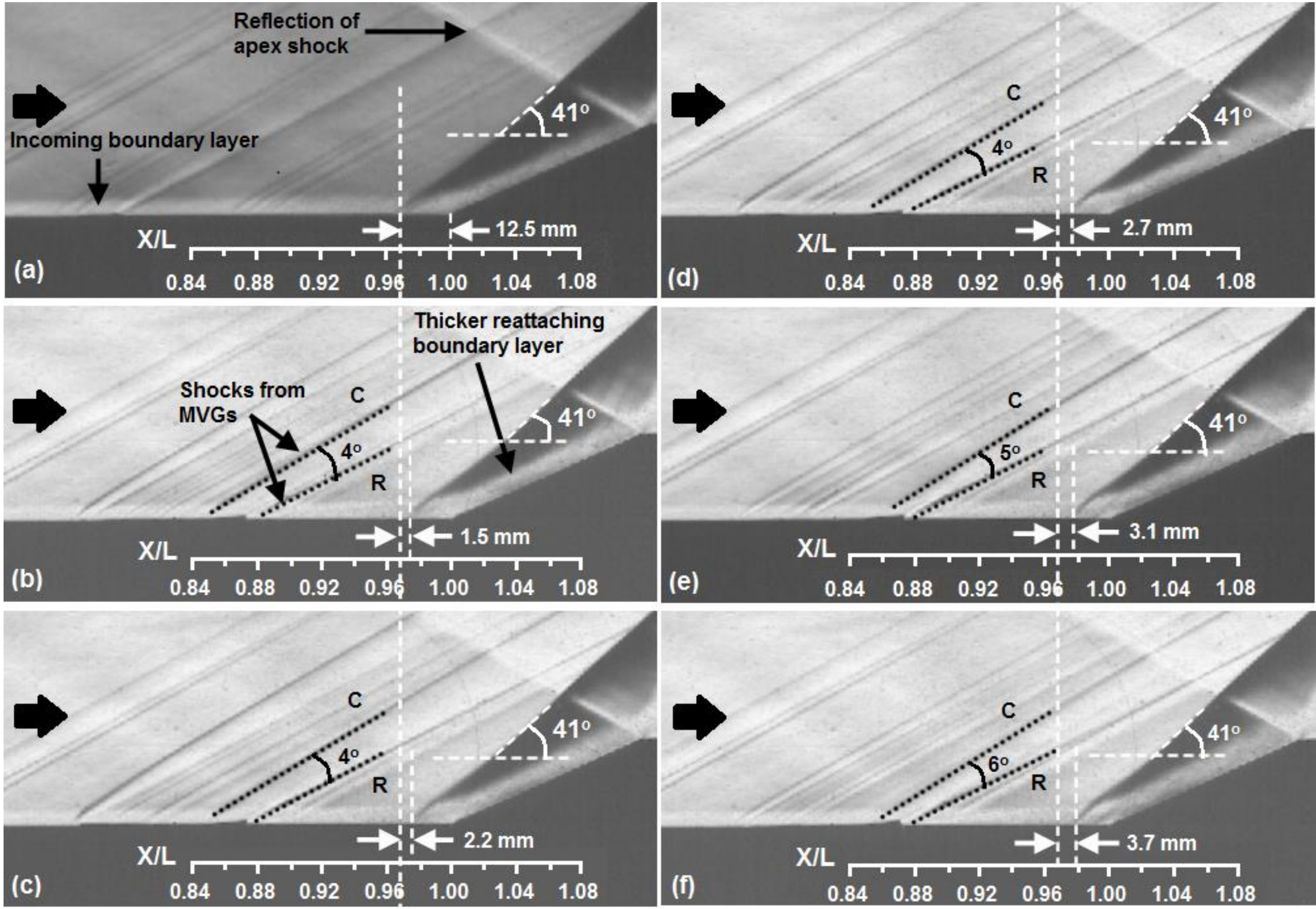

Surface pressure distributions

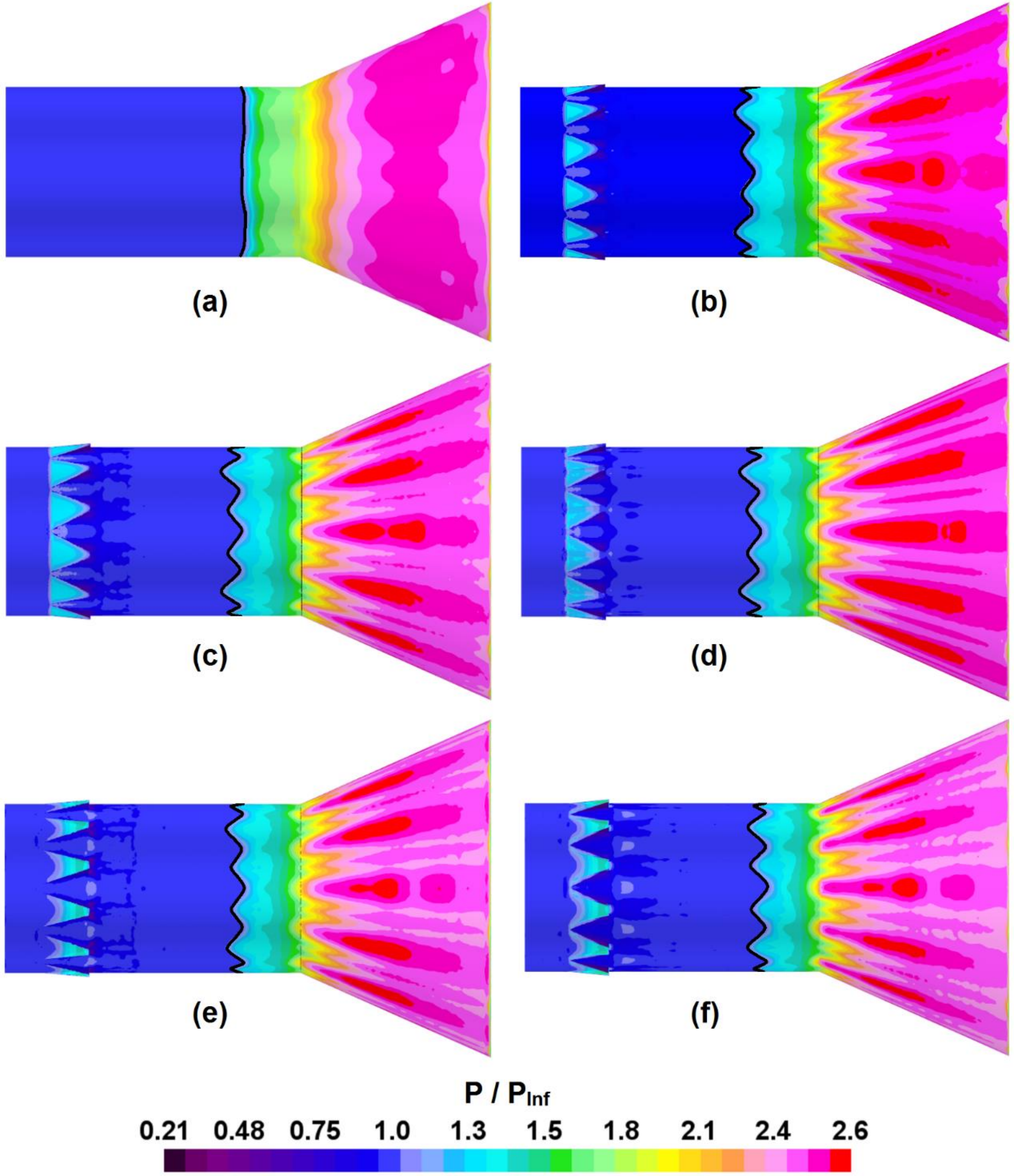

Average Upstream Influence Length (UI)

	MVG configuration	UI (mm)	UI / δ	UI / $UI_{(UC)}$
(a)	Uncontrolled (UC)	14.00	2.80	1.00
(b)	Baseline Ramp (BR)	18.50	3.70	1.32
(c)	Trapezoidal Ramp (TZ)	17.75	3.55	1.27
(d)	Split Ramp (SR)	17.00	3.40	1.21
(e)	Thick Vanes (TV)	16.75	3.35	1.20
(f)	Ramped Vanes (RV)	14.95	2.99	1.07

Separation shock's unsteadiness

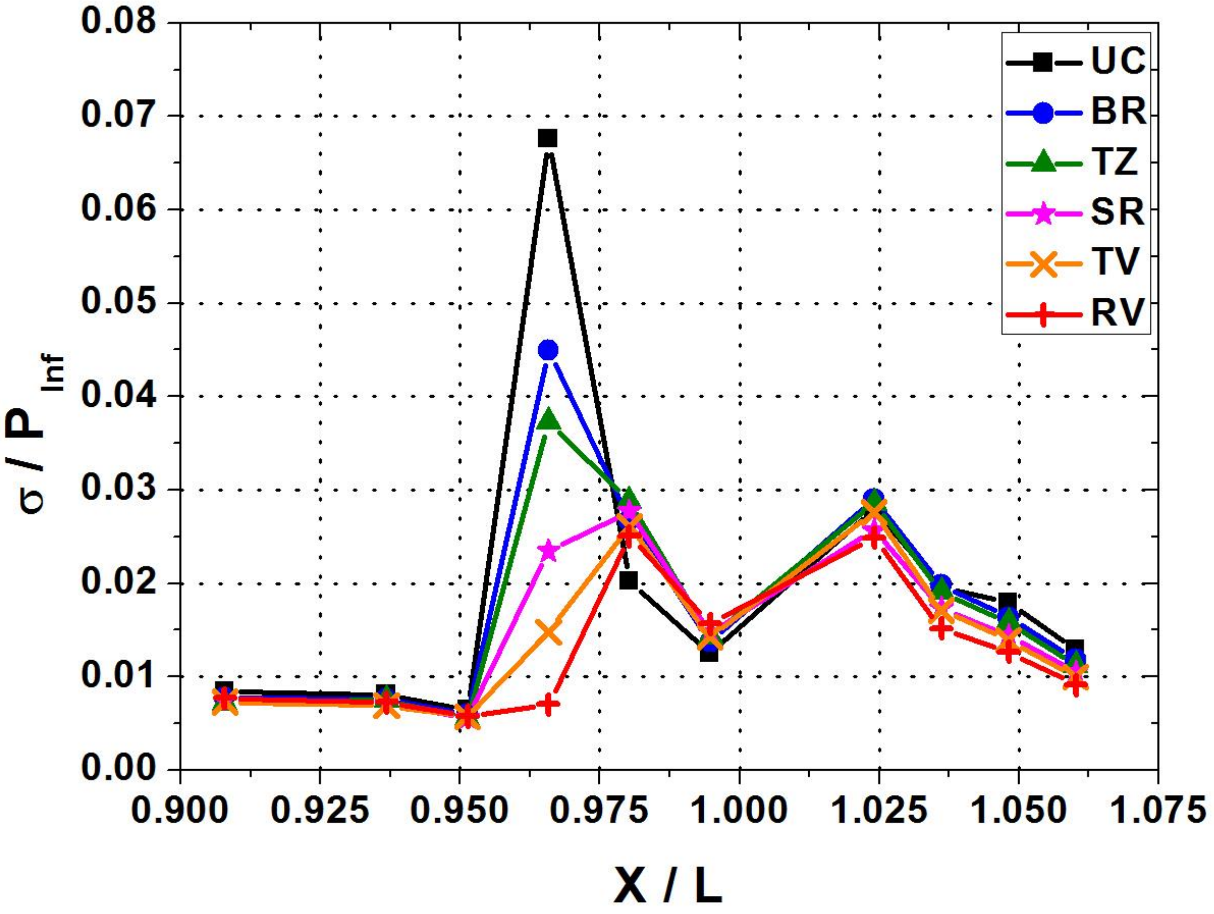

Standard deviation distributions

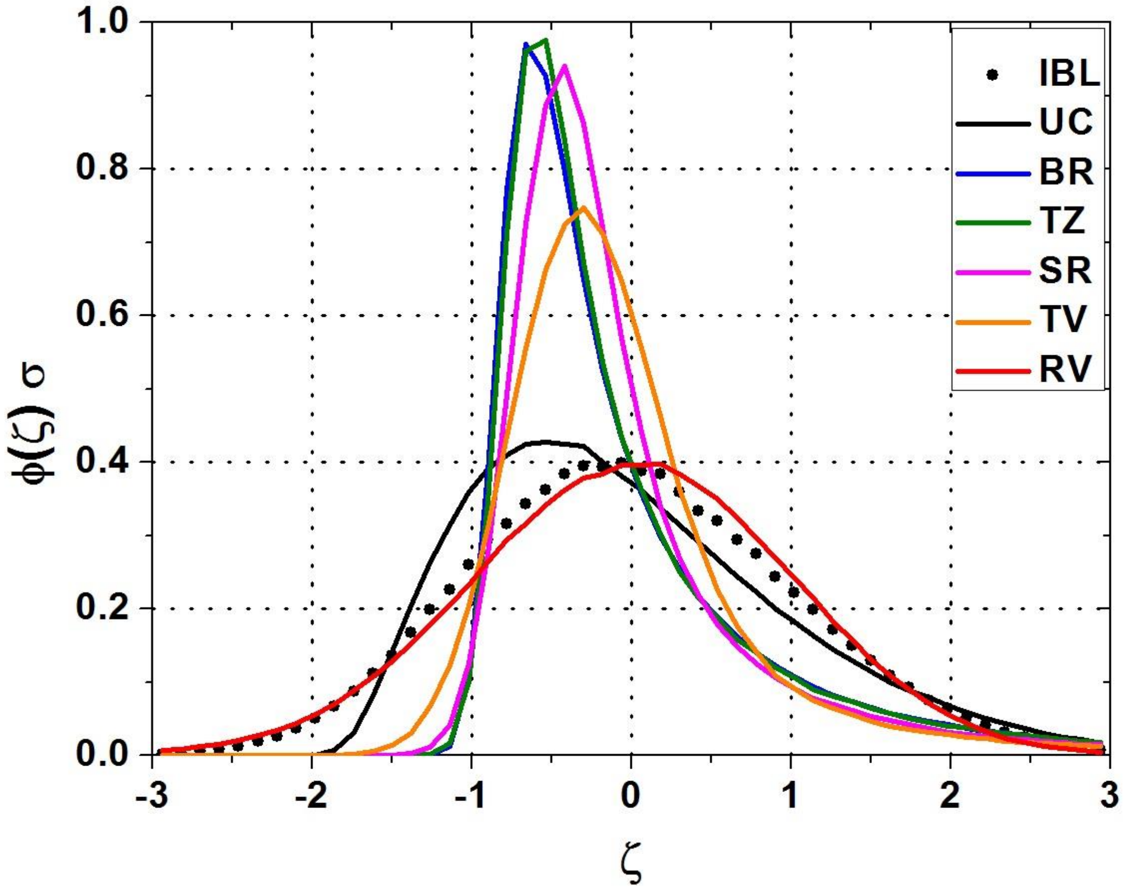

Probability Density Function (k4)

Separation shock's Intermittency

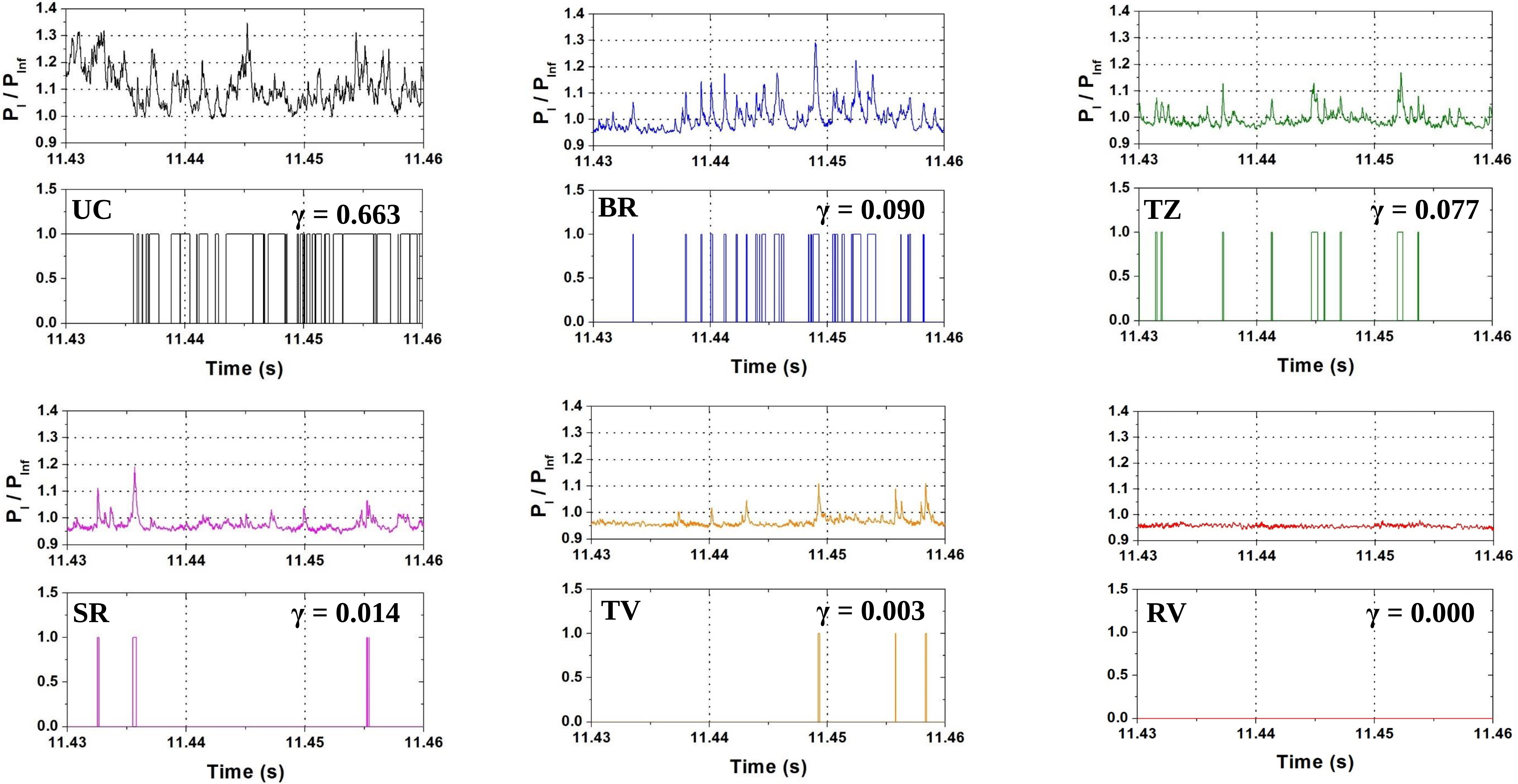

Power Spectral densities

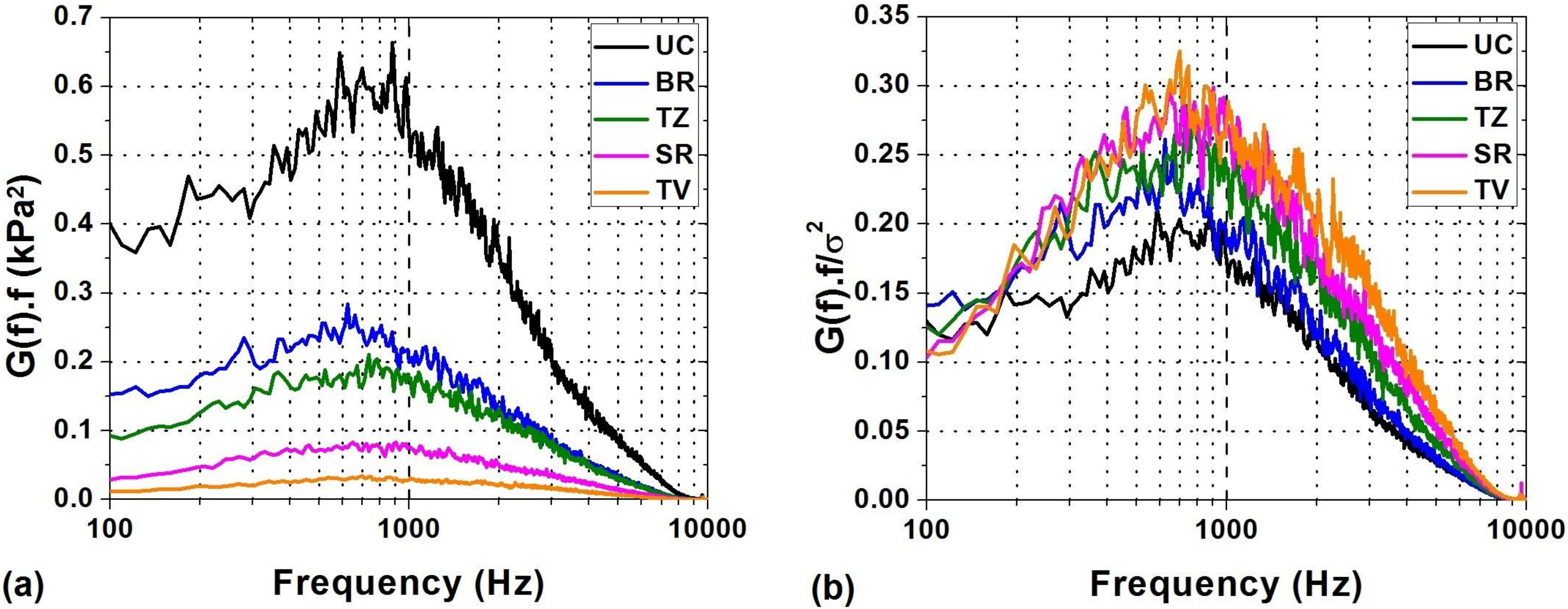

Comparison of power spectra (a) without normalization; (b) after normalization with respective variance (σ^2)

Separated flow topology

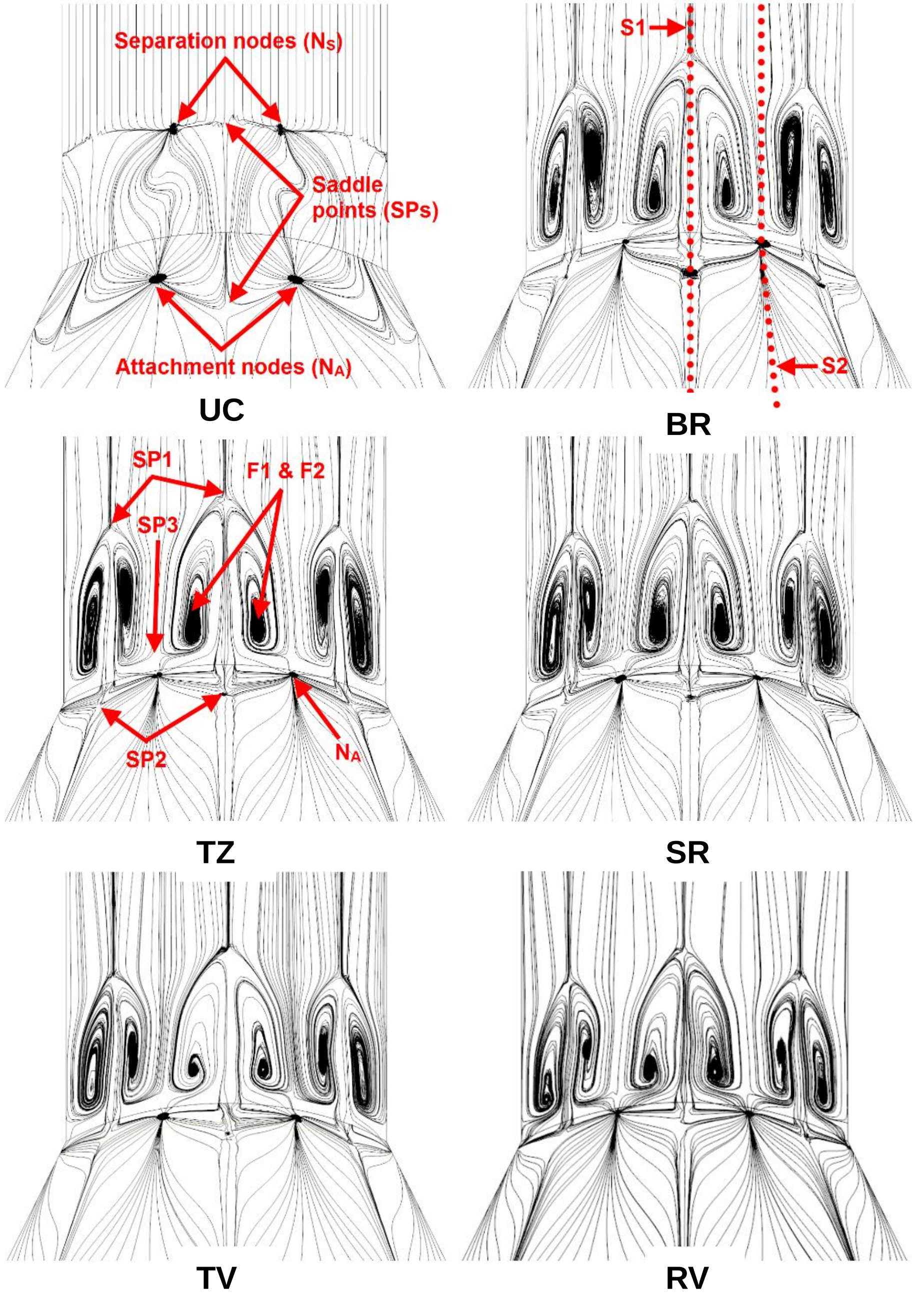

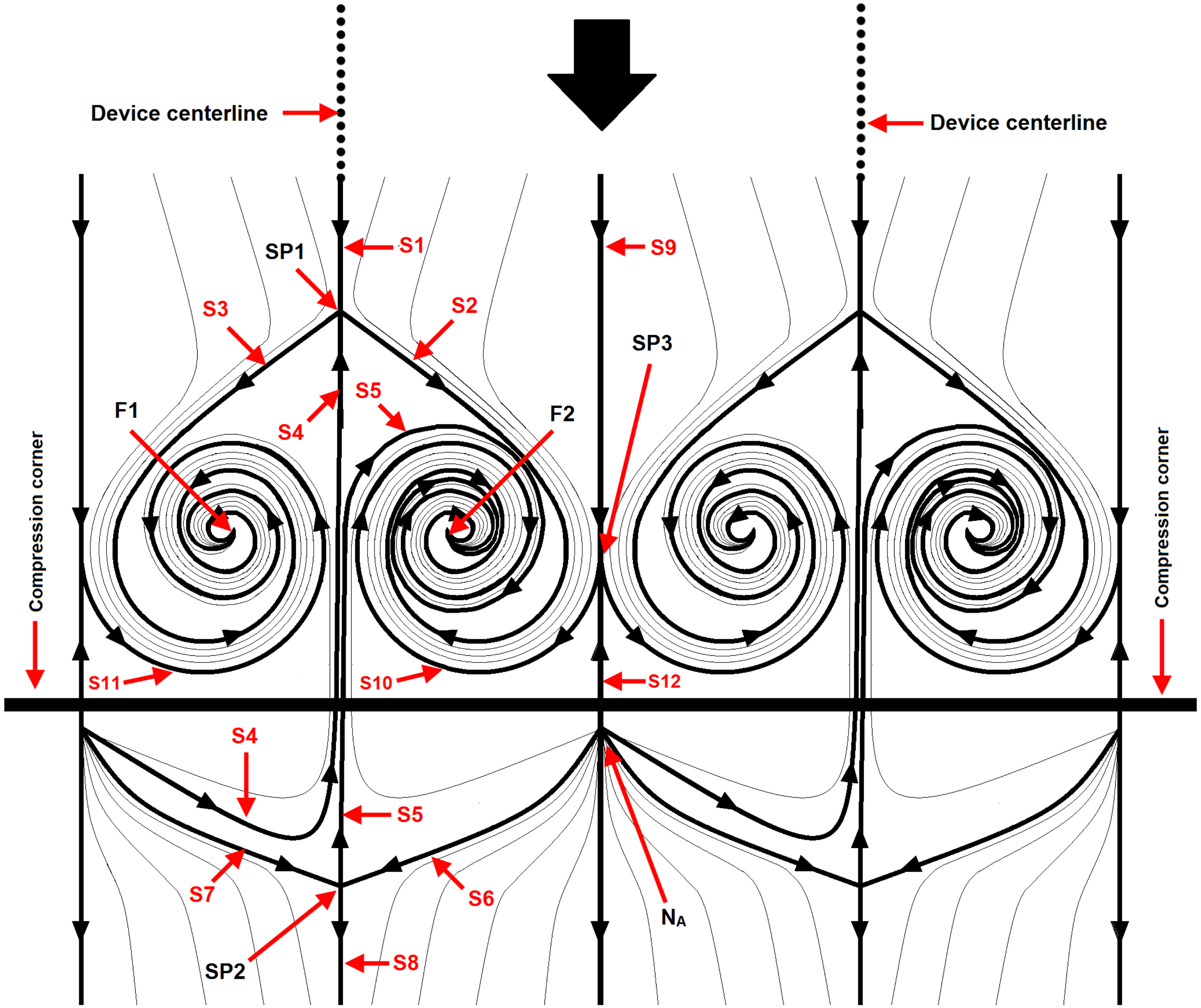

Flow assessment near the MVGs

(a) Baseline Ramp

(b) Trapezoidal Ramp

(c) Split Ramp

(d) Thick Vanes

(e) Ramped Vanes

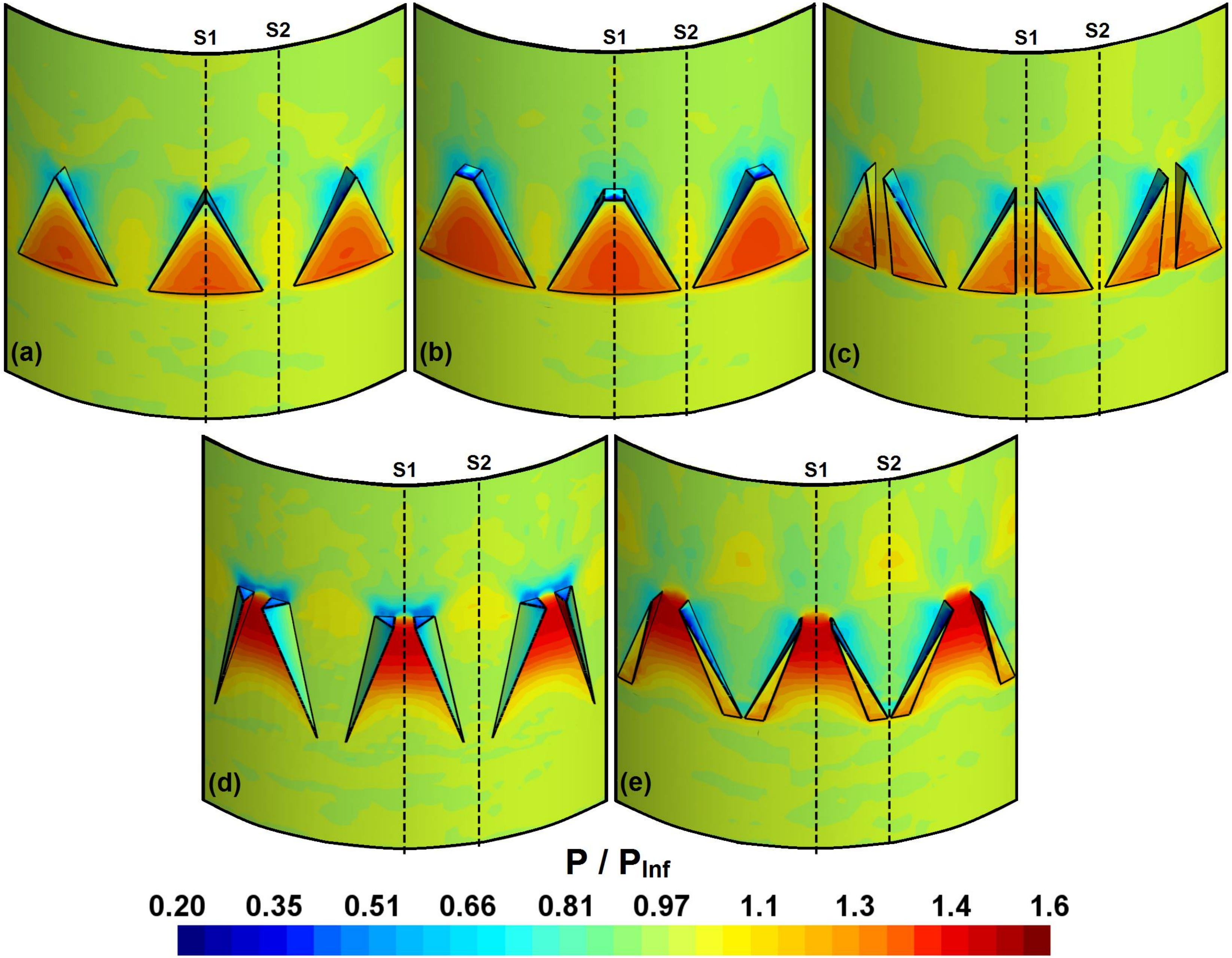

Streamwise vorticity distributions

(a) Baseline Ramp

(b) Trapezoidal Ramp

(c) Split Ramp

(d) Thick Vanes

(e) Ramped Vanes

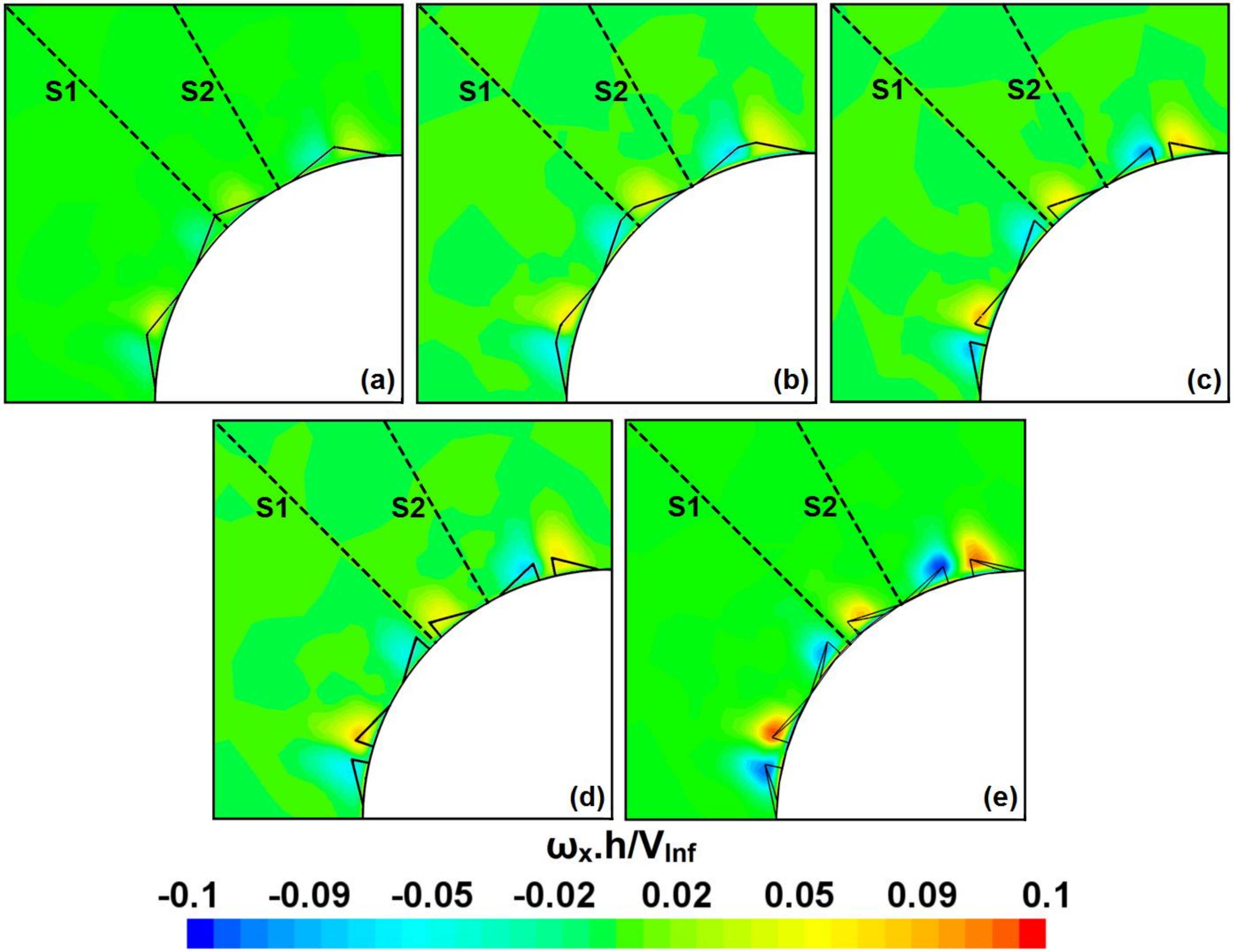

Relative velocity distributions

Relative velocity (V_R) is the difference between the streamwise velocity obtained from the uncontrolled and controlled interaction flowfields

$$V_R = V_{UC} - V_{RV}$$

(a) **Baseline Ramp**

(b) **Trapezoidal Ramp**

(c) **Split Ramp**

(d) **Thick Vanes**

(e) **Ramped Vanes**

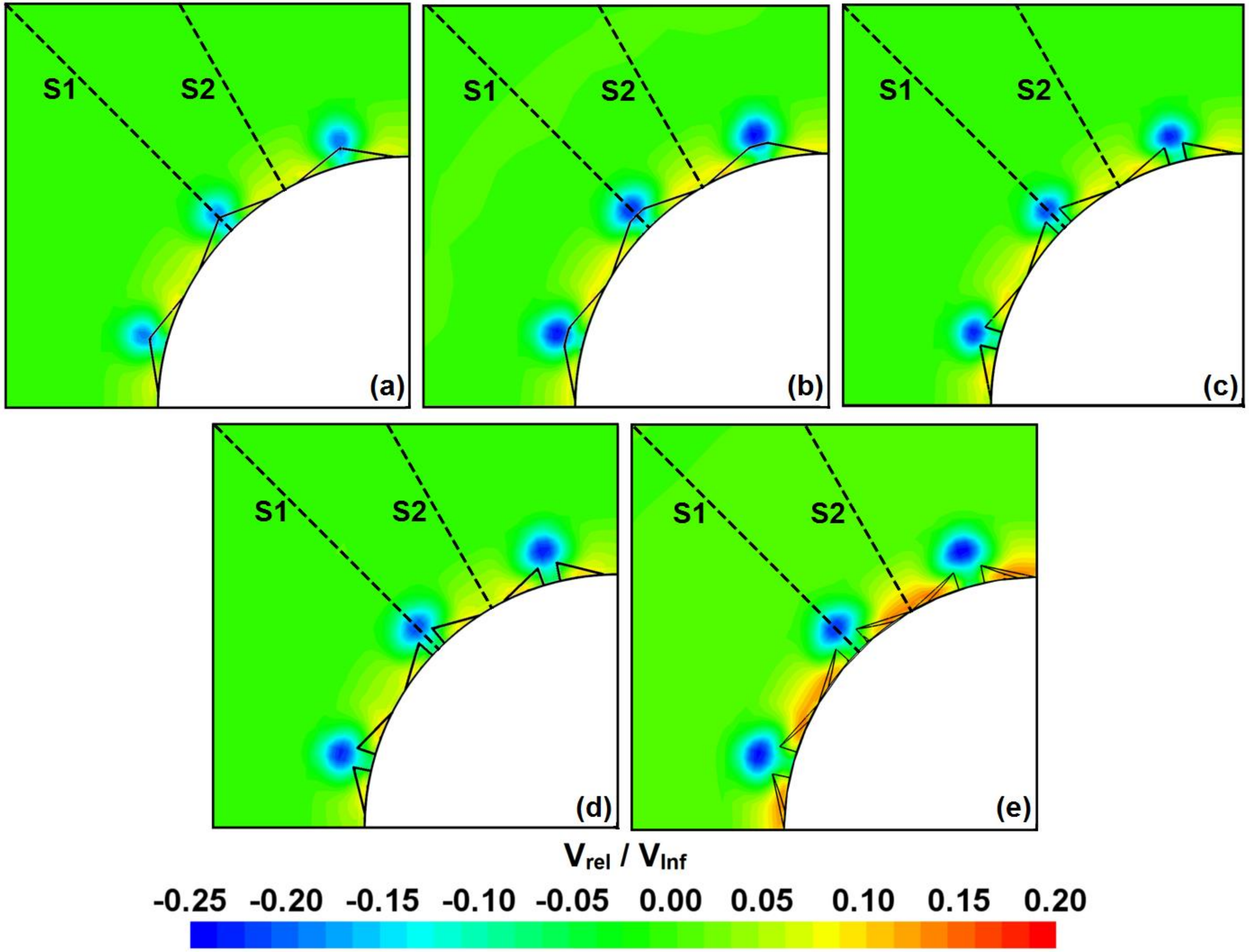

Assessment of MVG size

$$\pi d = n \; x \; 7.5h$$

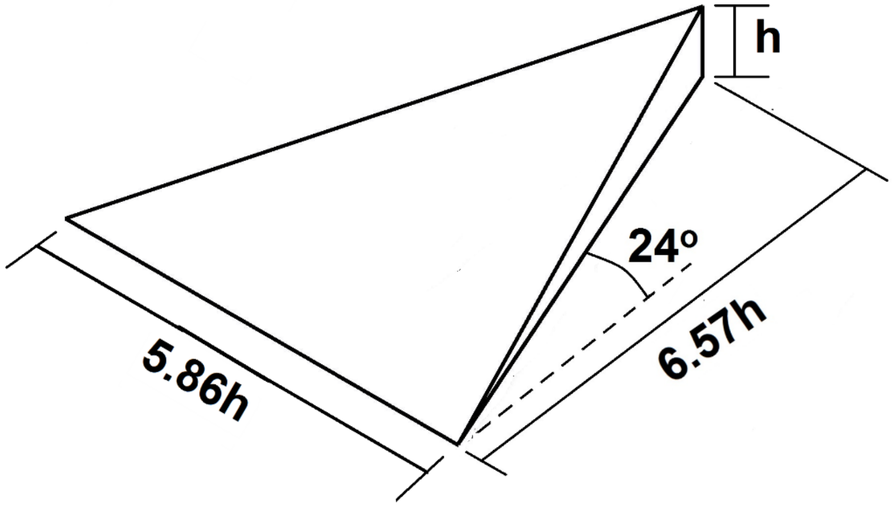

Baseline Ramp (BR)

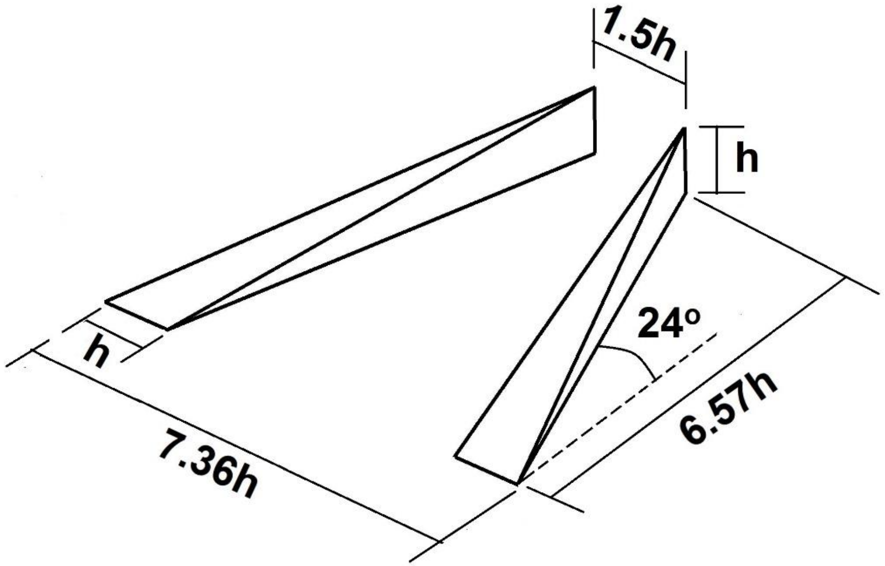

Ramped Vanes (RV)

n	h (mm)
4	4.2
5	3.4
6	**2.8**
7	2.4
8	**2.1**
9	1.9
10	1.7
11	1.5
12	**1.4**
13	1.3
14	1.2
15	1.1

Time-averaged Schlieren photographs

(a) Uncontrolled

(b) Baseline Ramp (h = 2.1 mm)

(c) Ramped Vanes (h = 2.1 mm)

(d) Baseline Ramp (h = 2.8 mm)

(e) Ramped Vanes (h = 2.8 mm)

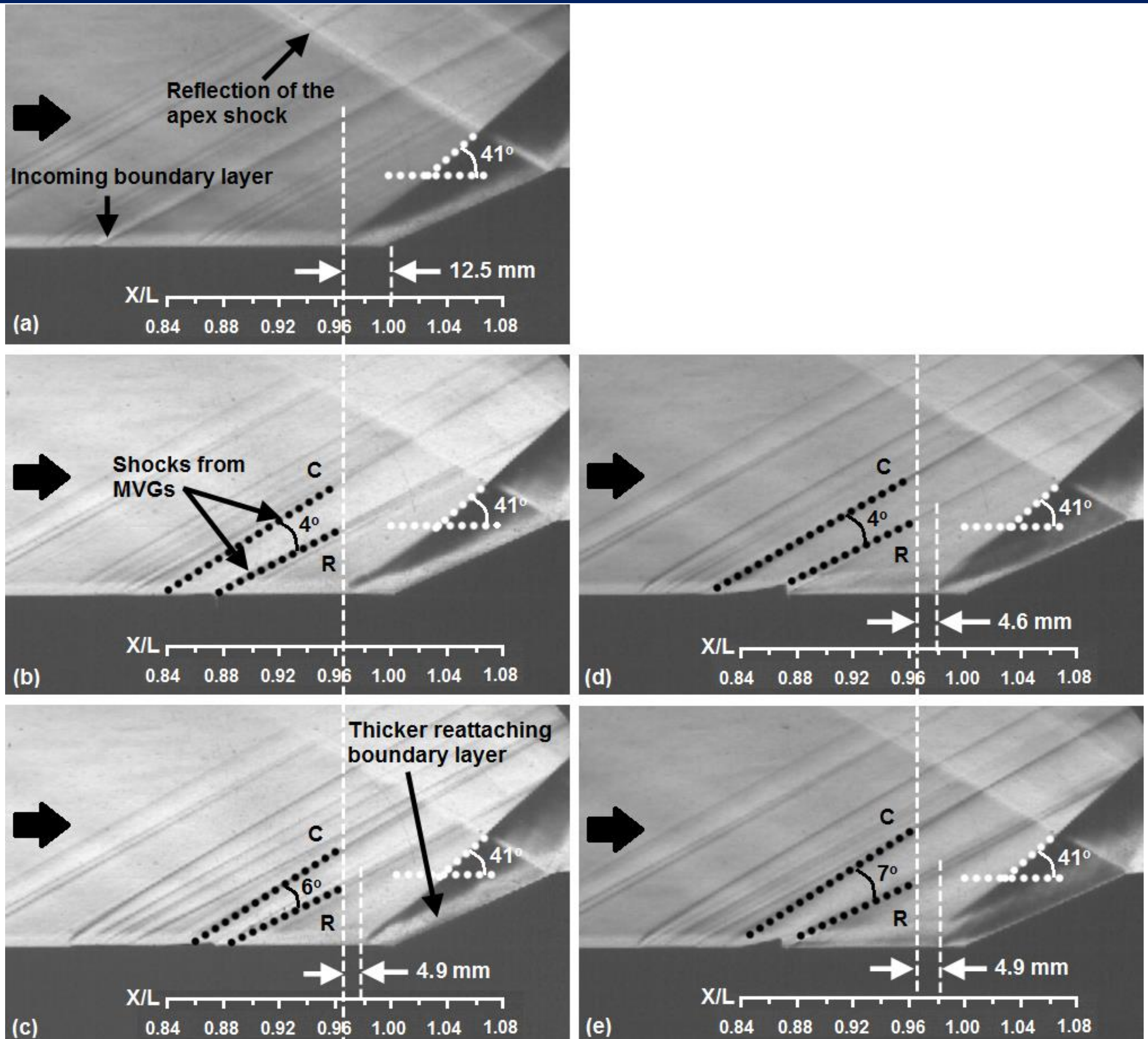

Surface flow topology

(a,b) Baseline Ramp (h = 2.1 mm)

(c,d) Ramped Vanes (h = 2.1 mm)

(e,f) Baseline Ramp (h = 2.8 mm)

(g,h) Ramped Vanes (h = 2.8 mm

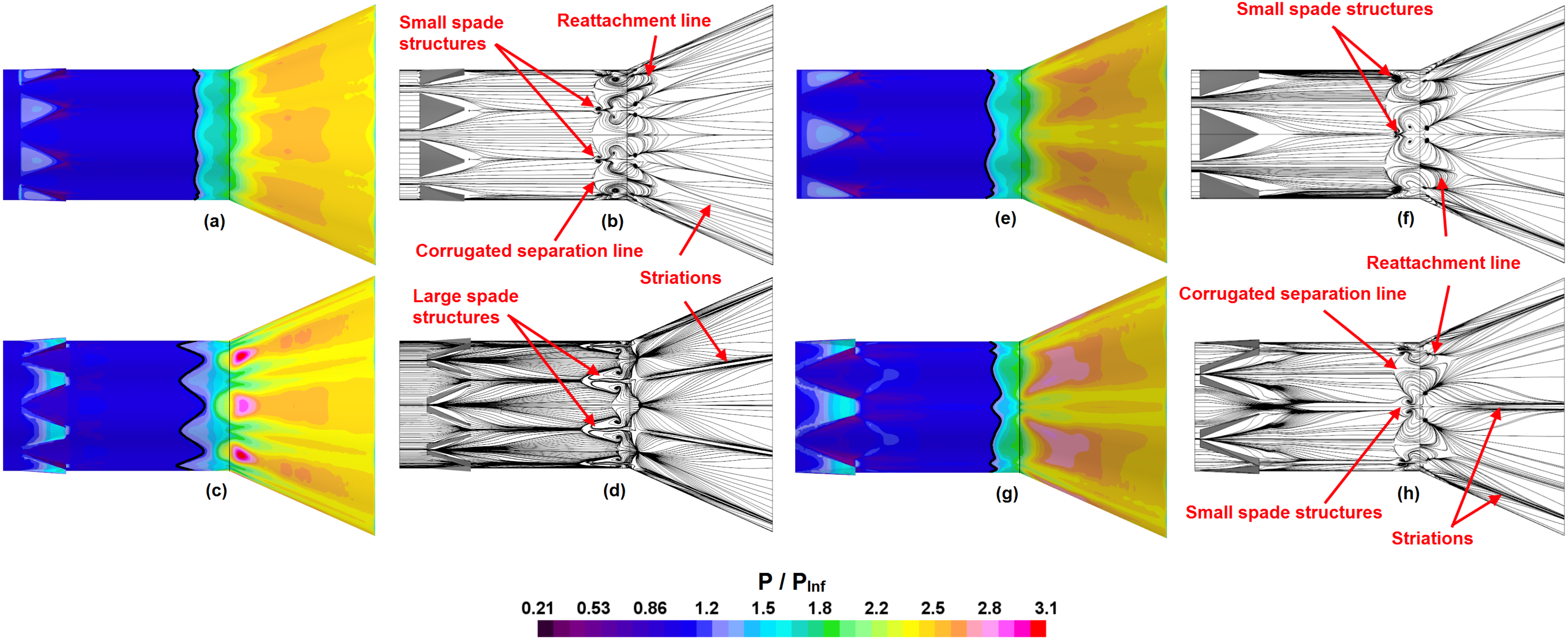

Surface flow topology

Average upstream influence length (UI)

Configuration	(UI)	UI / UI_{UC}
UC (UI_{UC})	2.8 δ	1.00
BR21	2.7 δ	0.96
RV21	2.9 δ	1.04
BR28	2.4 δ	0.86
RV28	1.8 δ	0.64

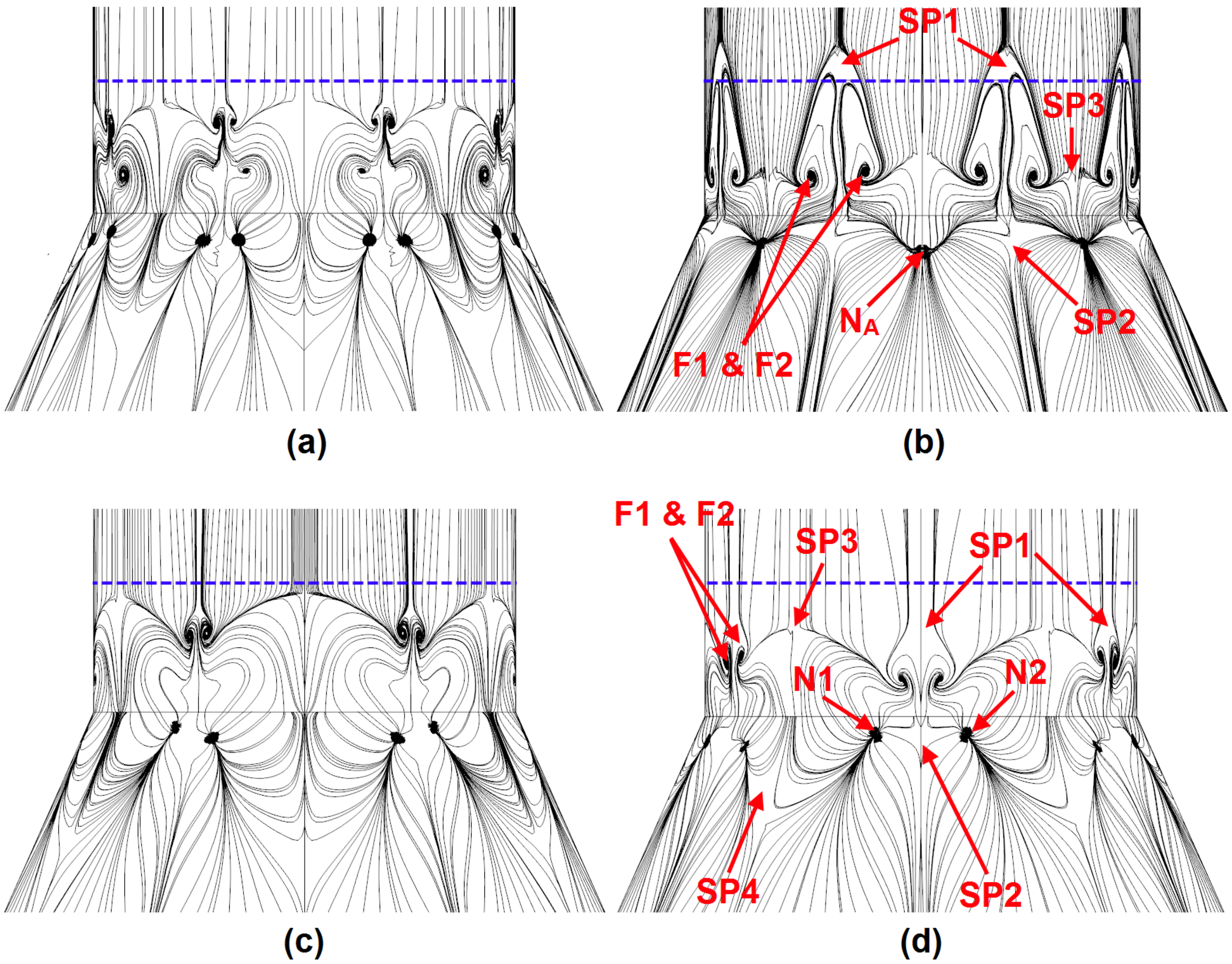

(a) Baseline Ramp (h = 2.1 mm)

(b) Ramped Vanes (h = 2.1 mm)

(c) Baseline Ramp (h = 2.8 mm)

(d) Ramped Vanes (h = 2.8 mm)

Kulite position and Standard deviation distributions

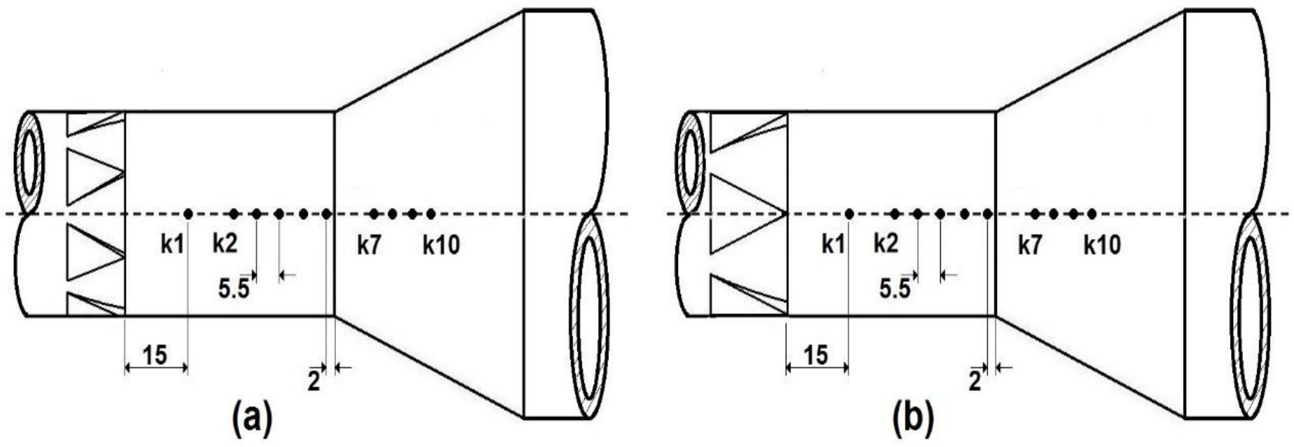

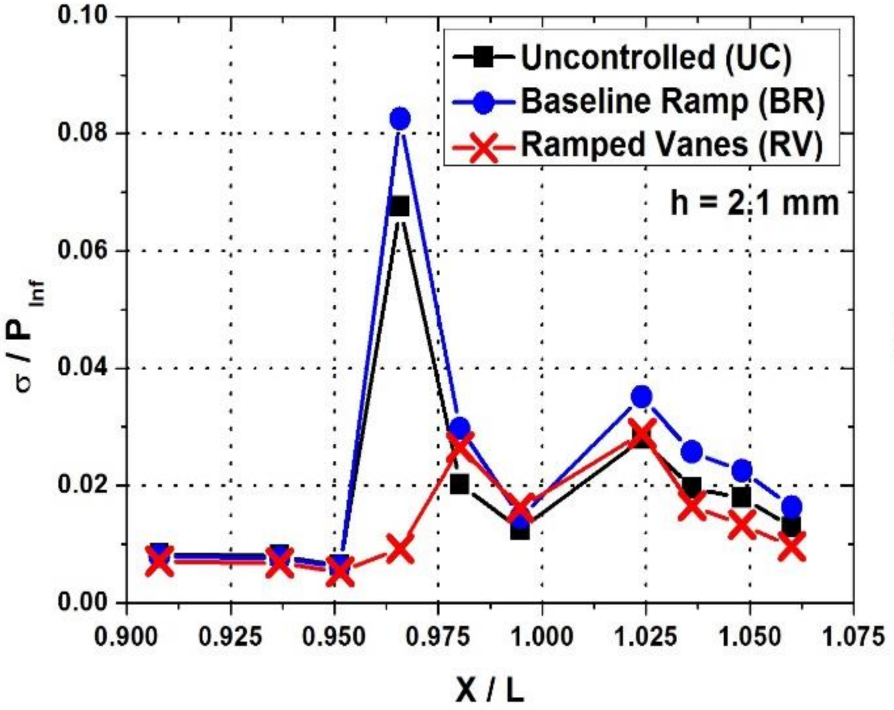

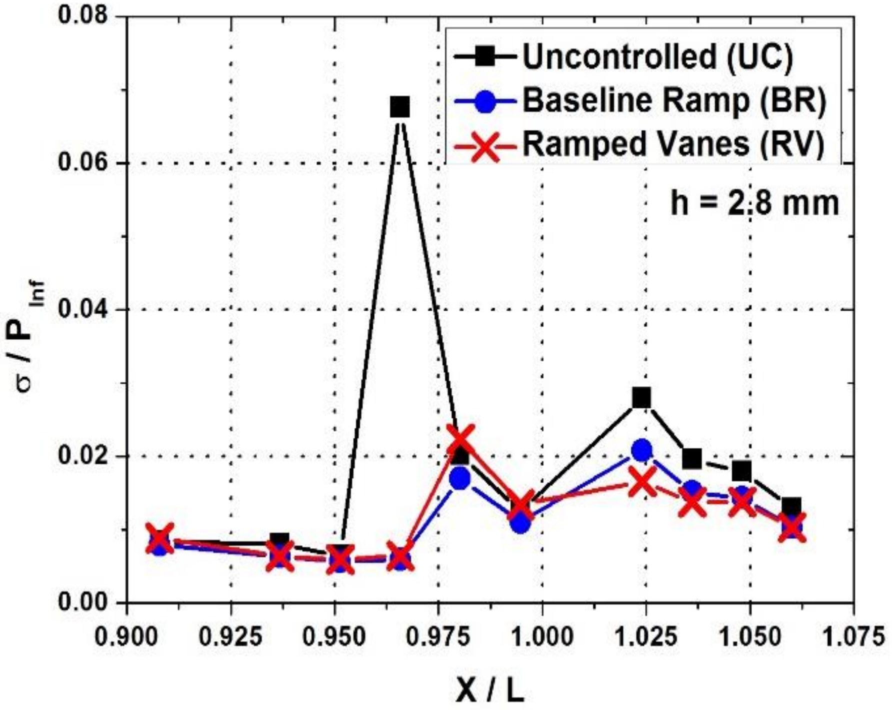

Separation shock’s unsteadiness across k4 (h = 2.1 mm)

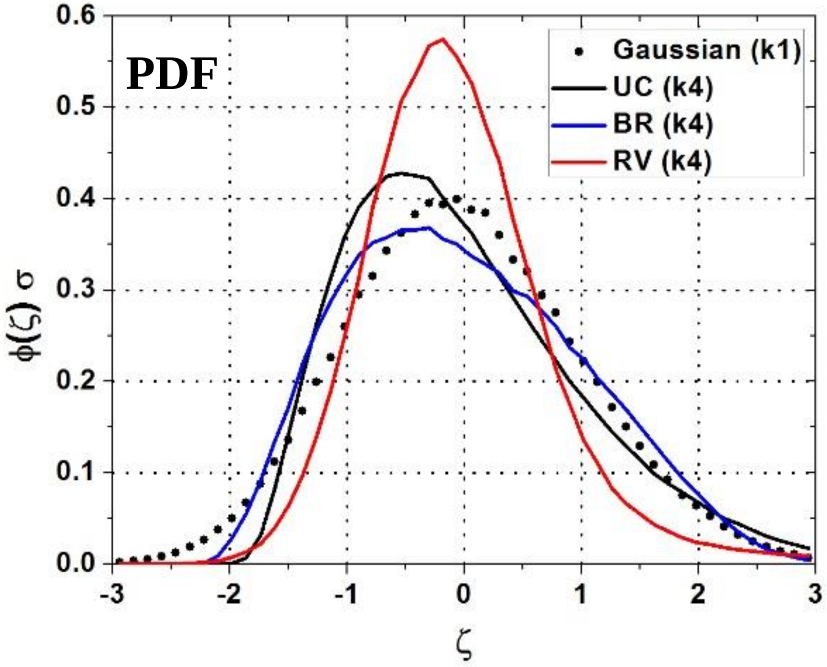

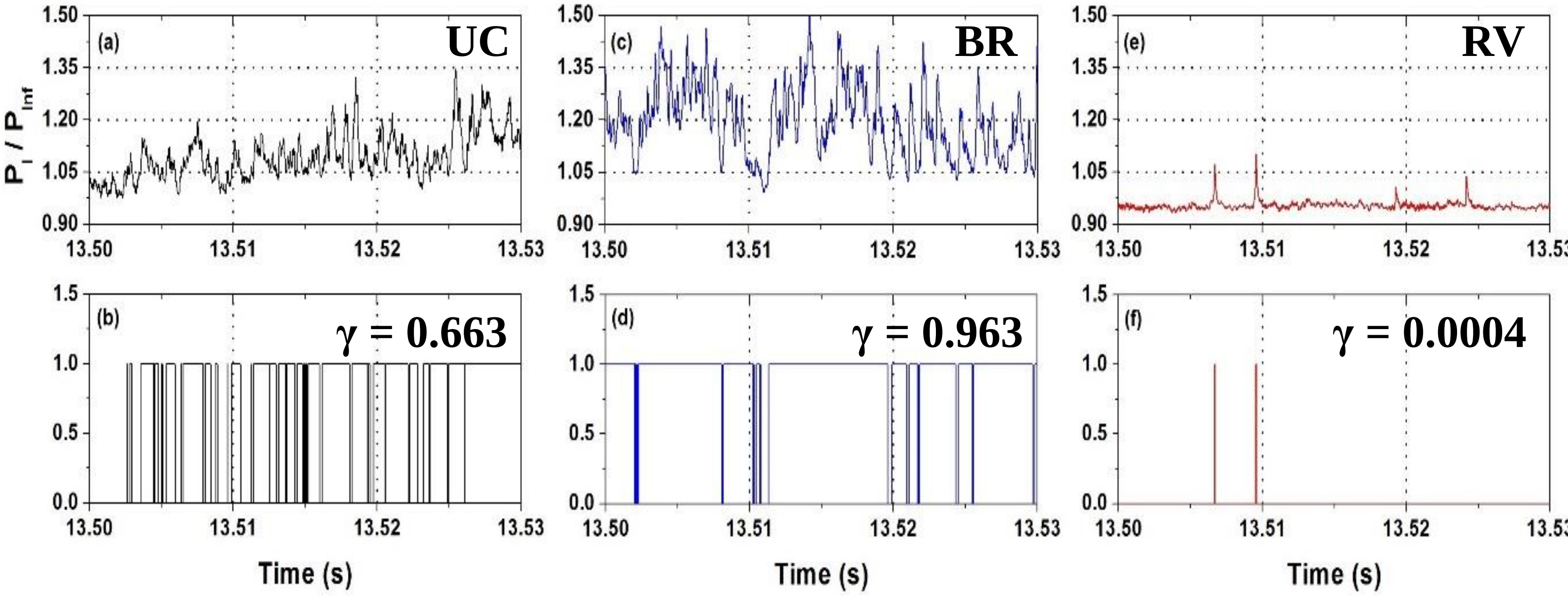

Real-time and box-car signals

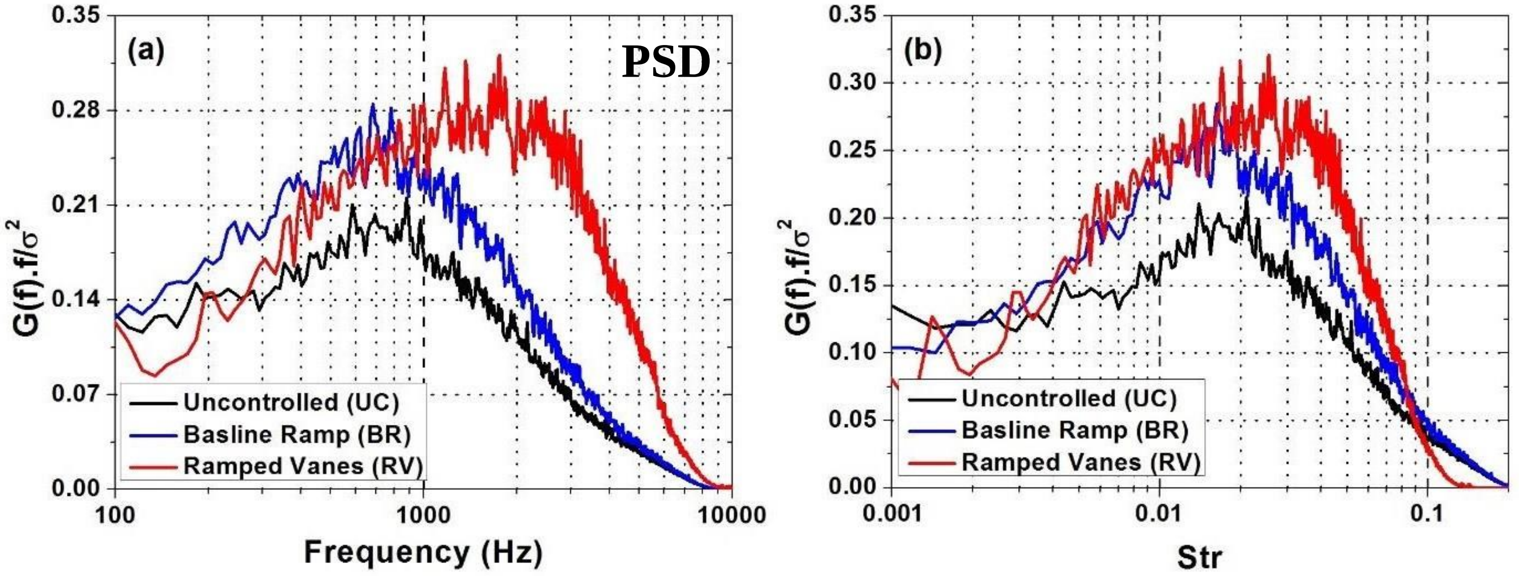

- For the uncontrolled case, the Shock frequency was in the range of 0.55 kHz to 0.9 kHz
- RVs of h = 2.1 mm increased this frequency to 1.1 kHz to 1.7 kHz along the downwash region, which is a significant and beneficial outcome

Streamwise vorticity and relative velocity distributions

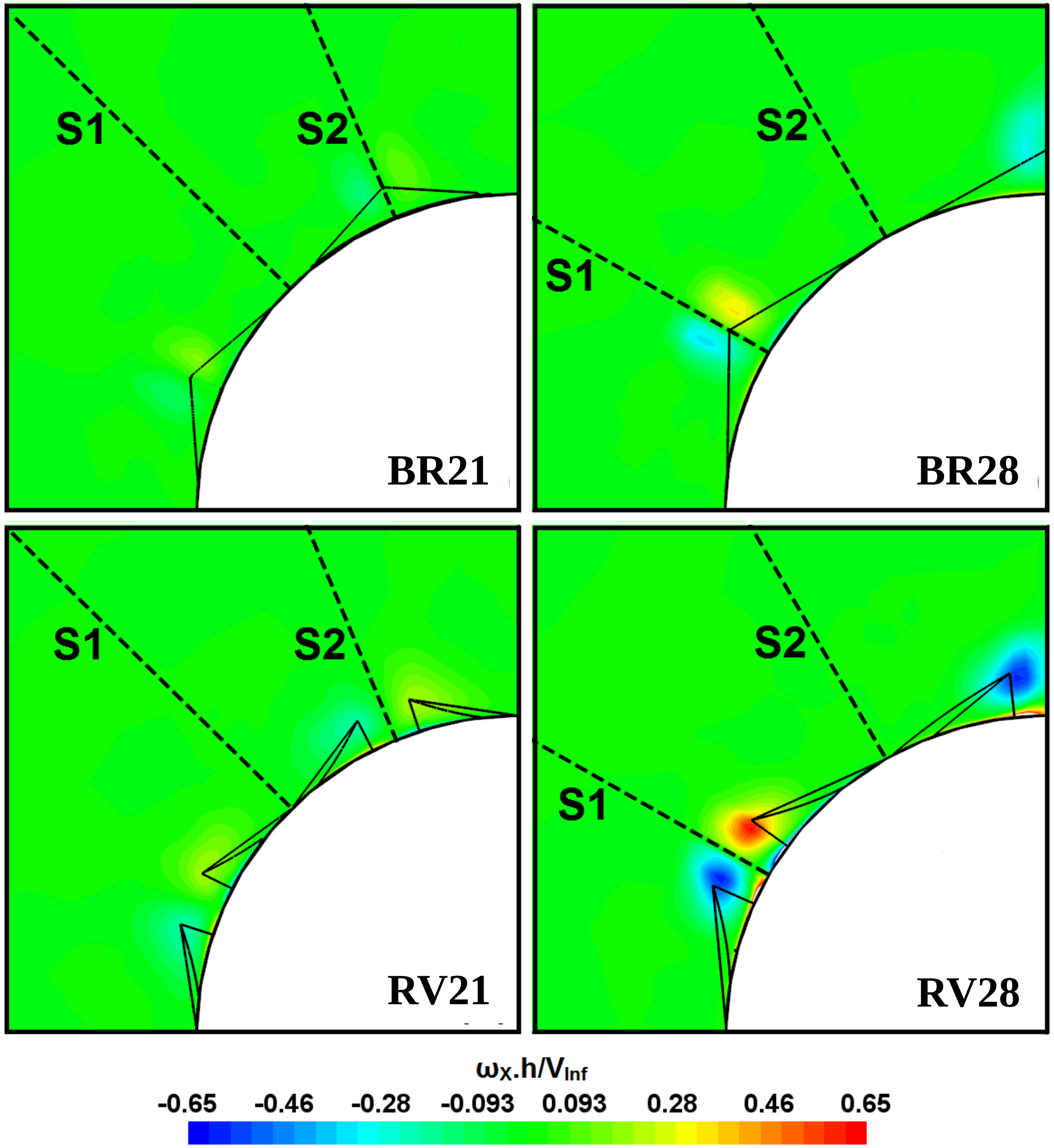

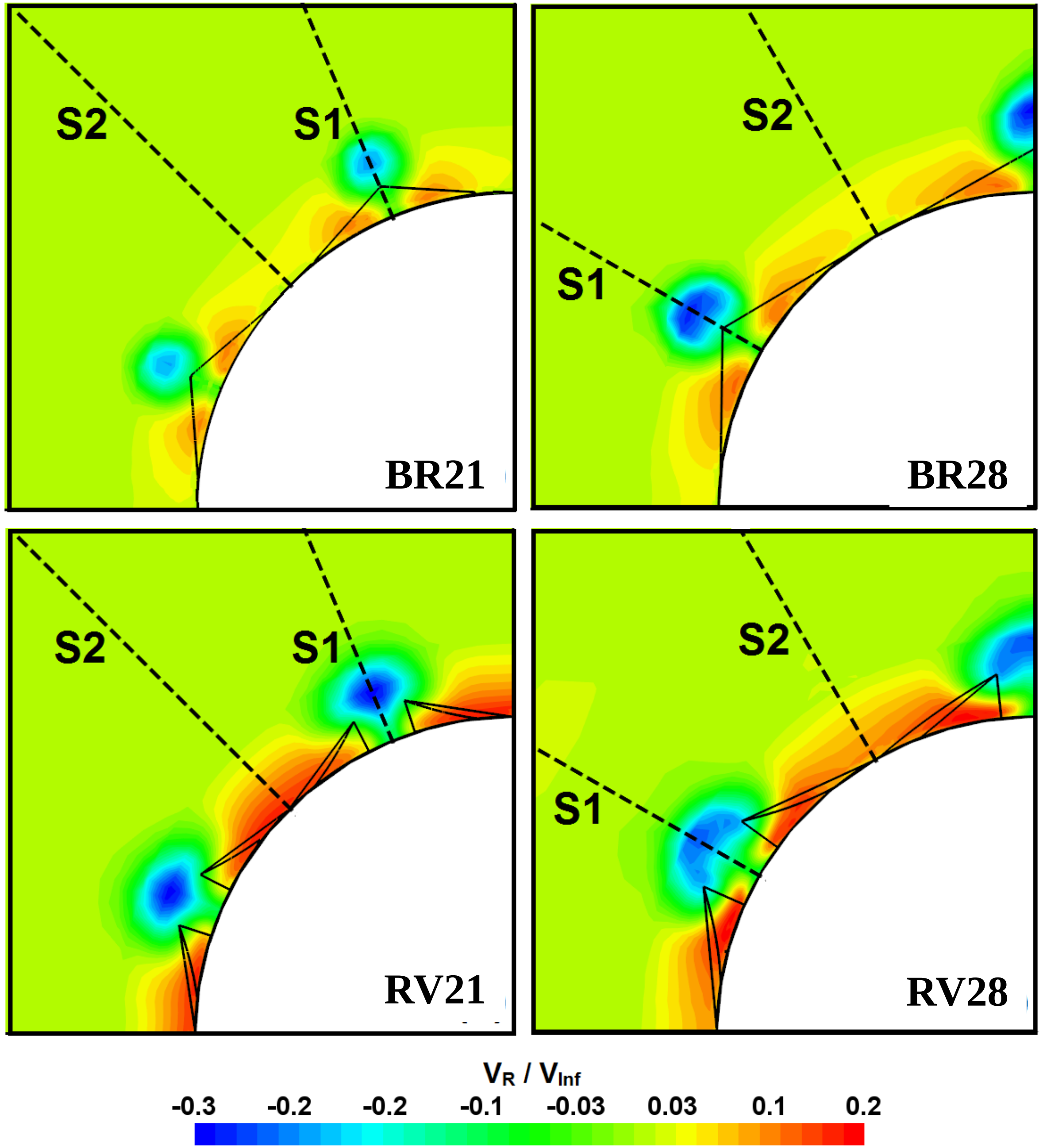

Effect of trailing edge height – Ramped Vanes

- h = 1.4 mm, 2.1 mm and 2.8 mm
- Inter-device spacing = 7.5h (10.5 mm)
- Trailing edge gap = 3h (4.2 mm)
- Streamwise length = 6.57h (9.2 mm)

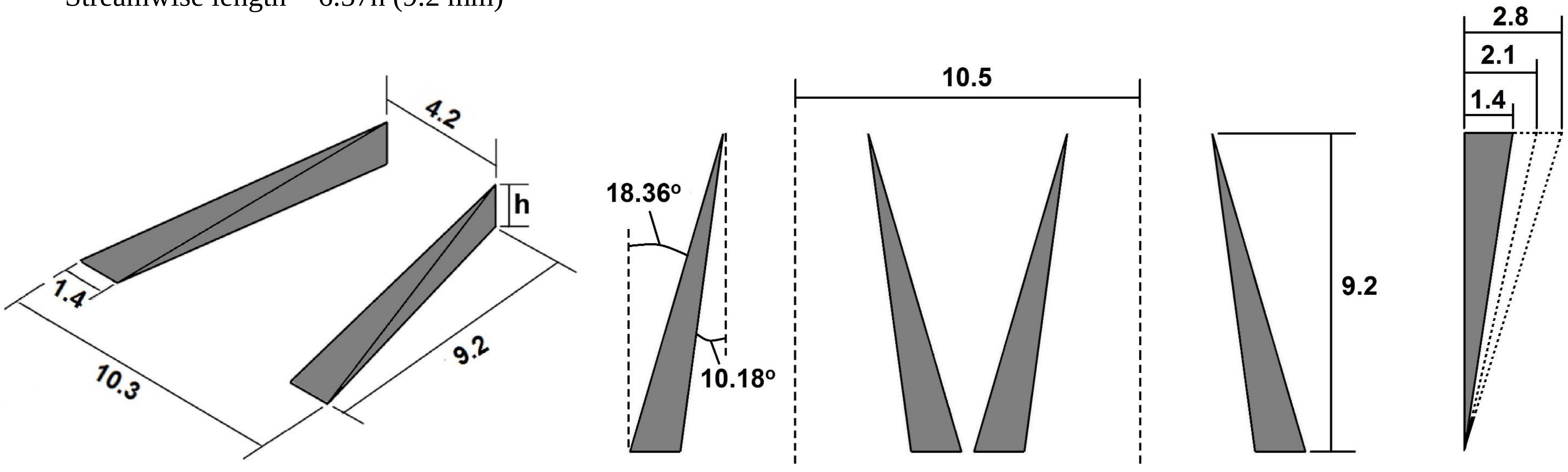

(a) (b) (c)

Schlieren visualizations

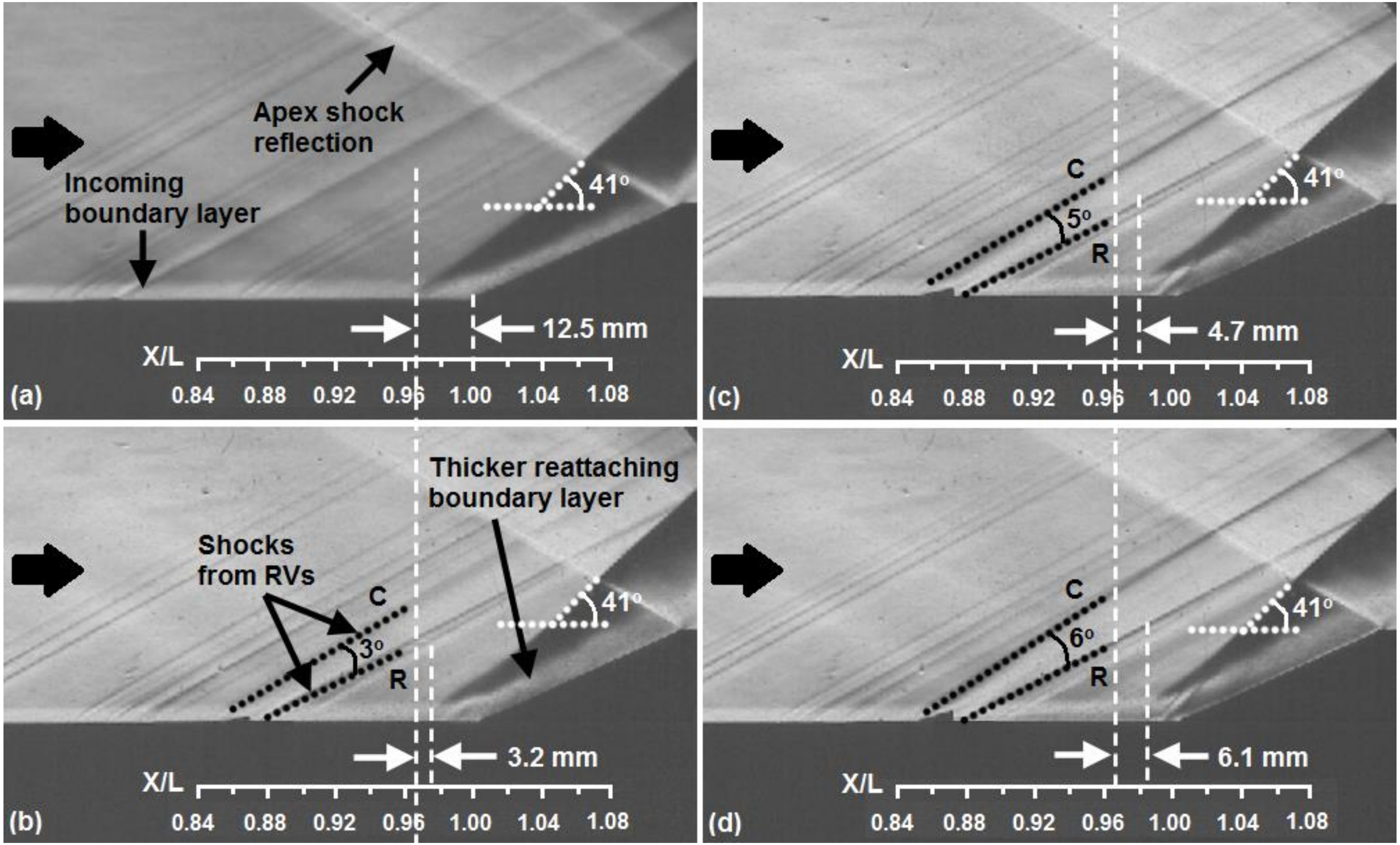

(a) Uncontrolled; (b) h = 1.4 mm; (c) h = 2.1 mm; (d) h = 2.8 mm

Numerical surface flow topology

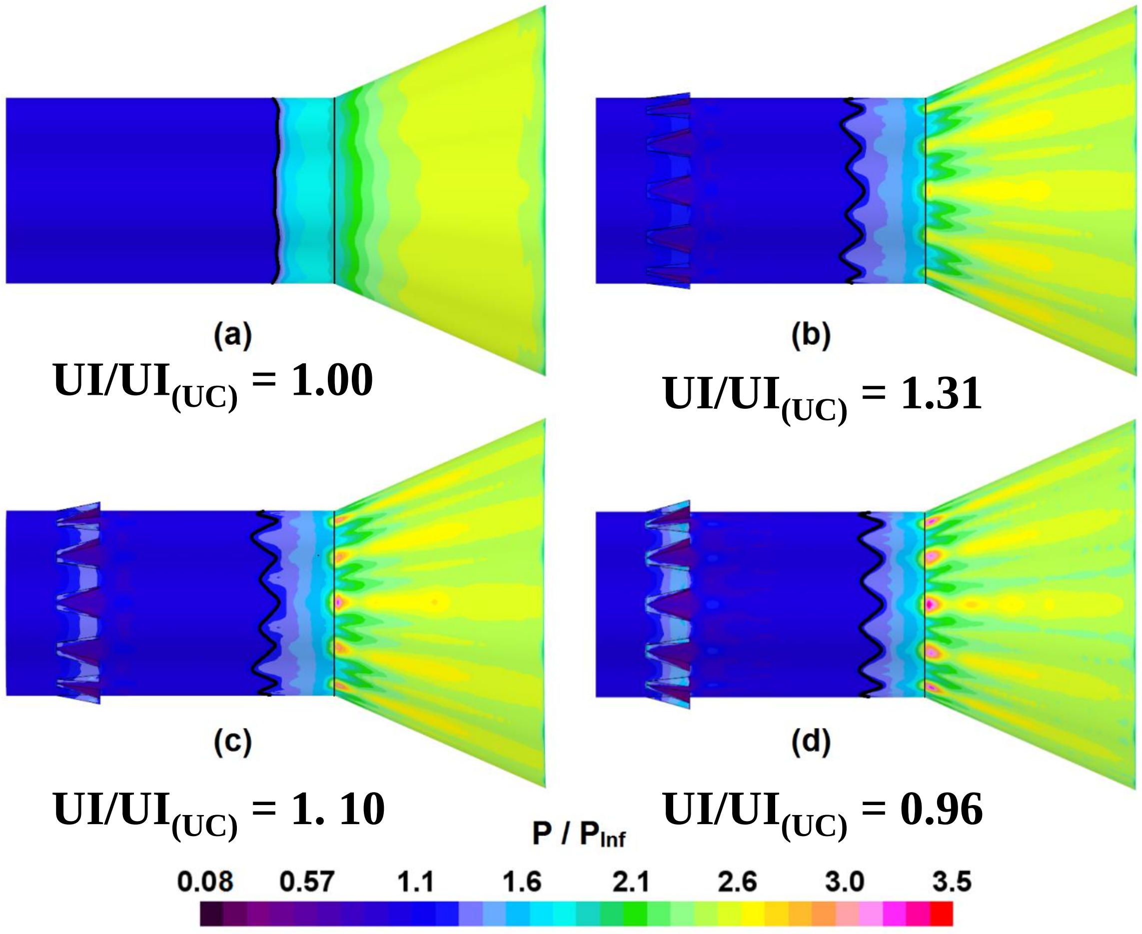

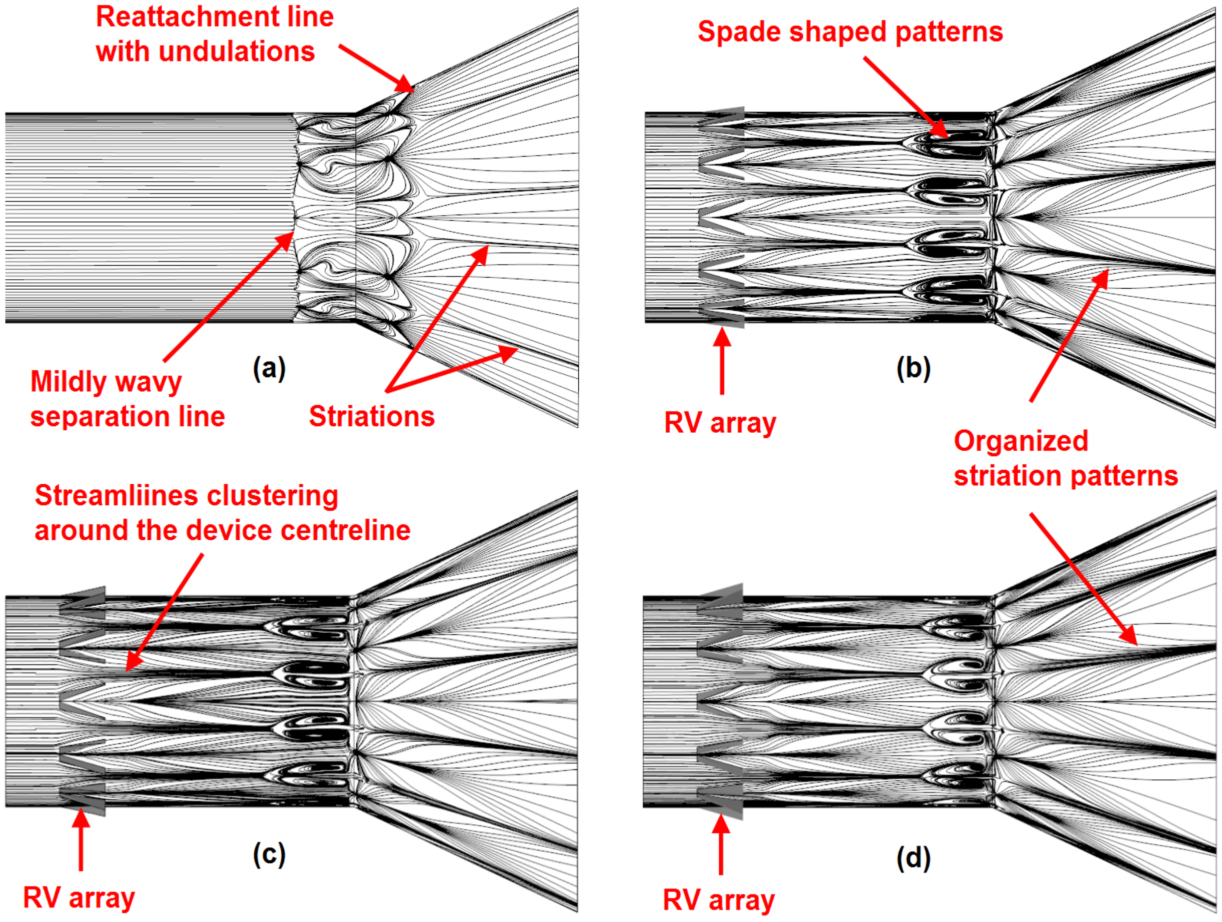

(a) Uncontrolled; (b) h = 1.4 mm; (c) h = 2.1 mm; (d) h = 2.8 mm

Surface oil flow visualizations – Controlled interactions

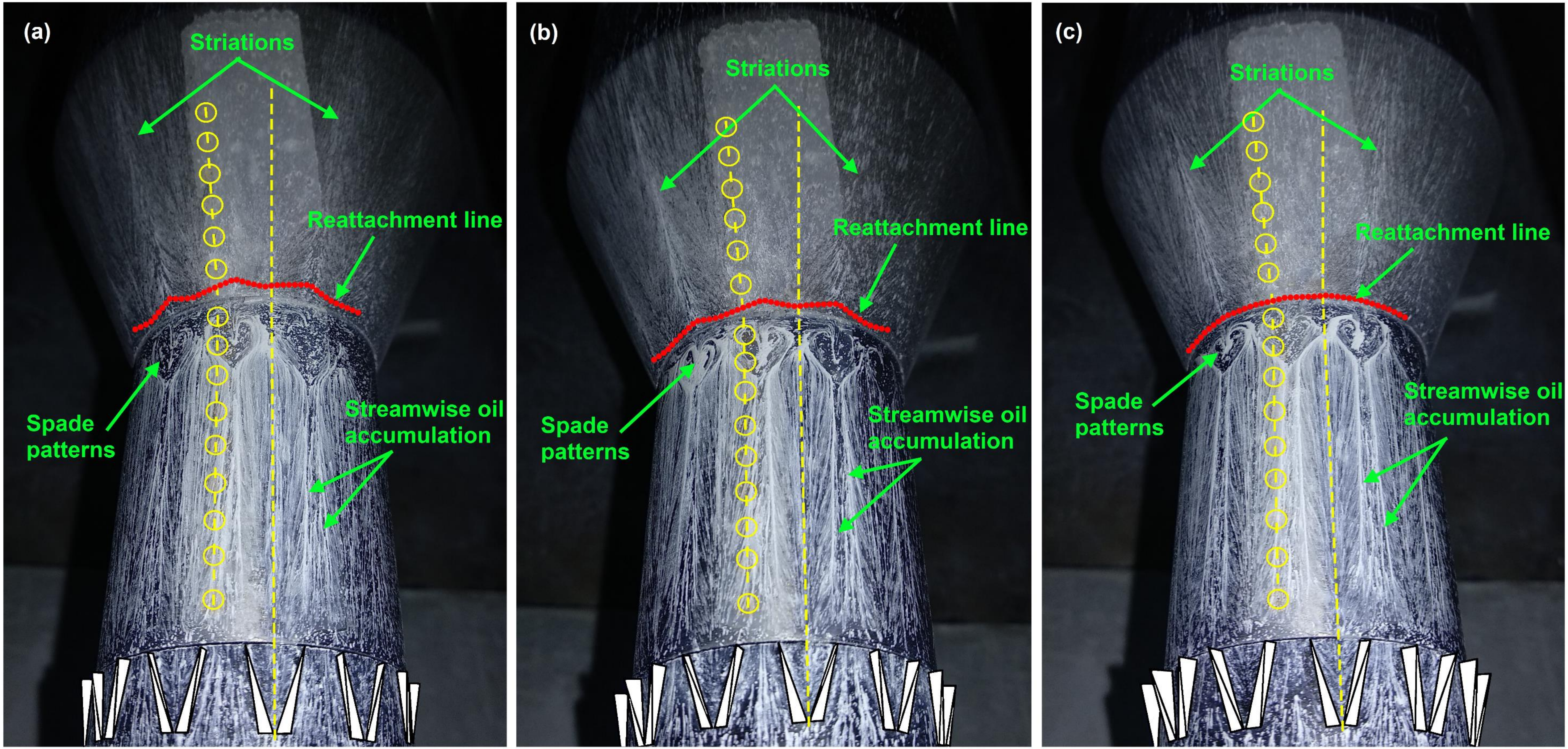

(a) h = 1.4 mm; (b) h = 2.1 mm and (c) h = 2.8 mm

Critical points and separation length

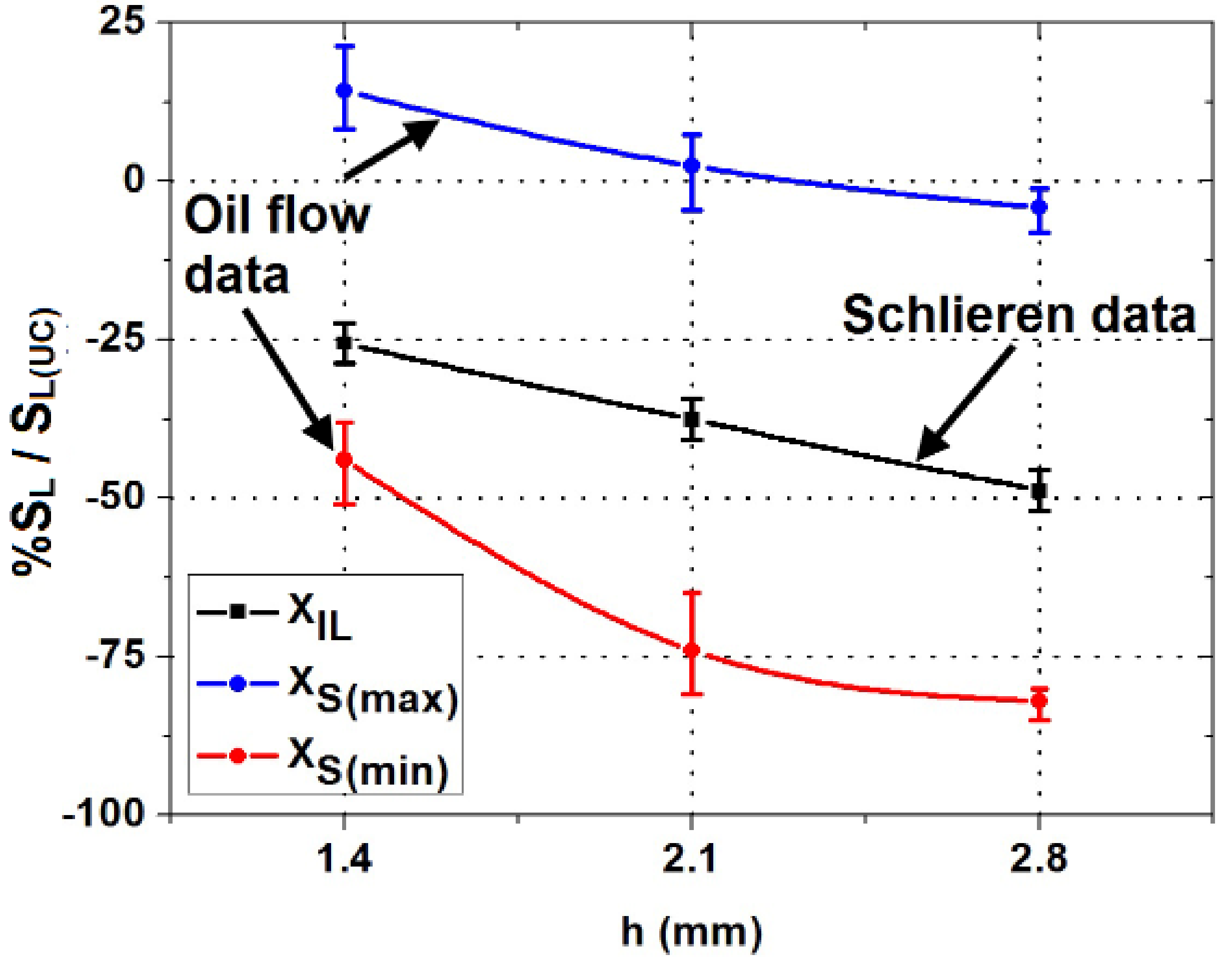

Interaction & separation lengths

h = 1.4 mm

h = 2.1 mm

h = 2.8 mm

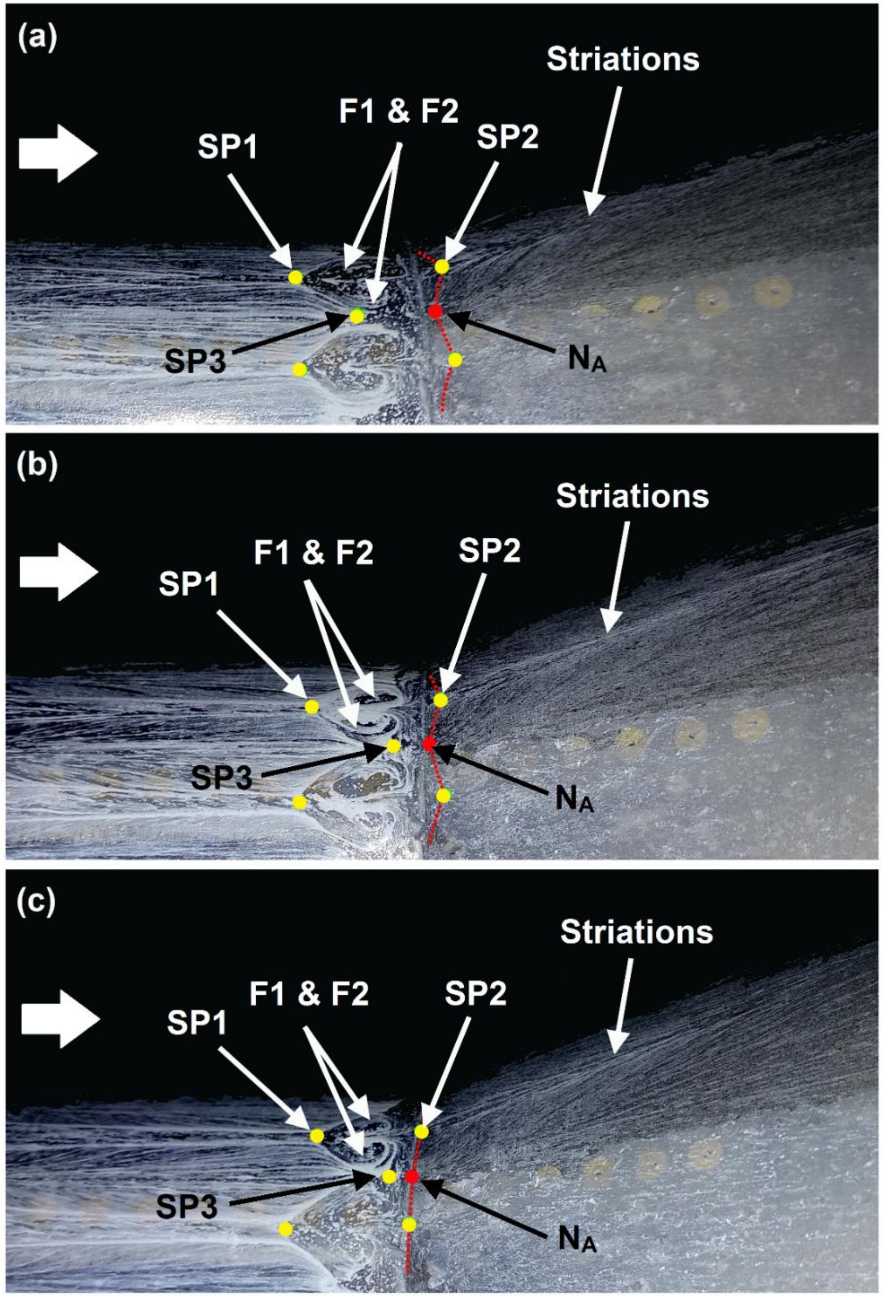

Intermittent characteristics of the separation shock

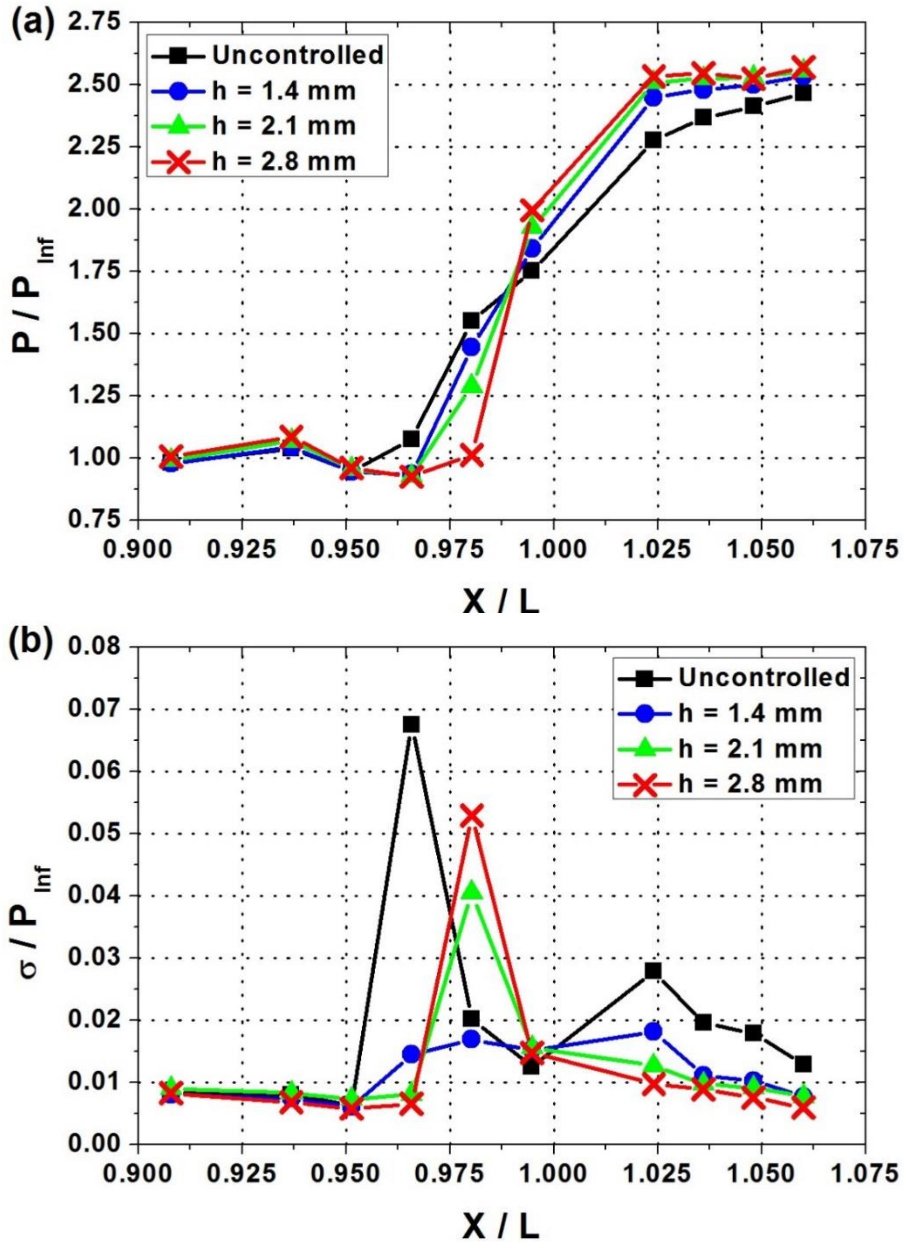

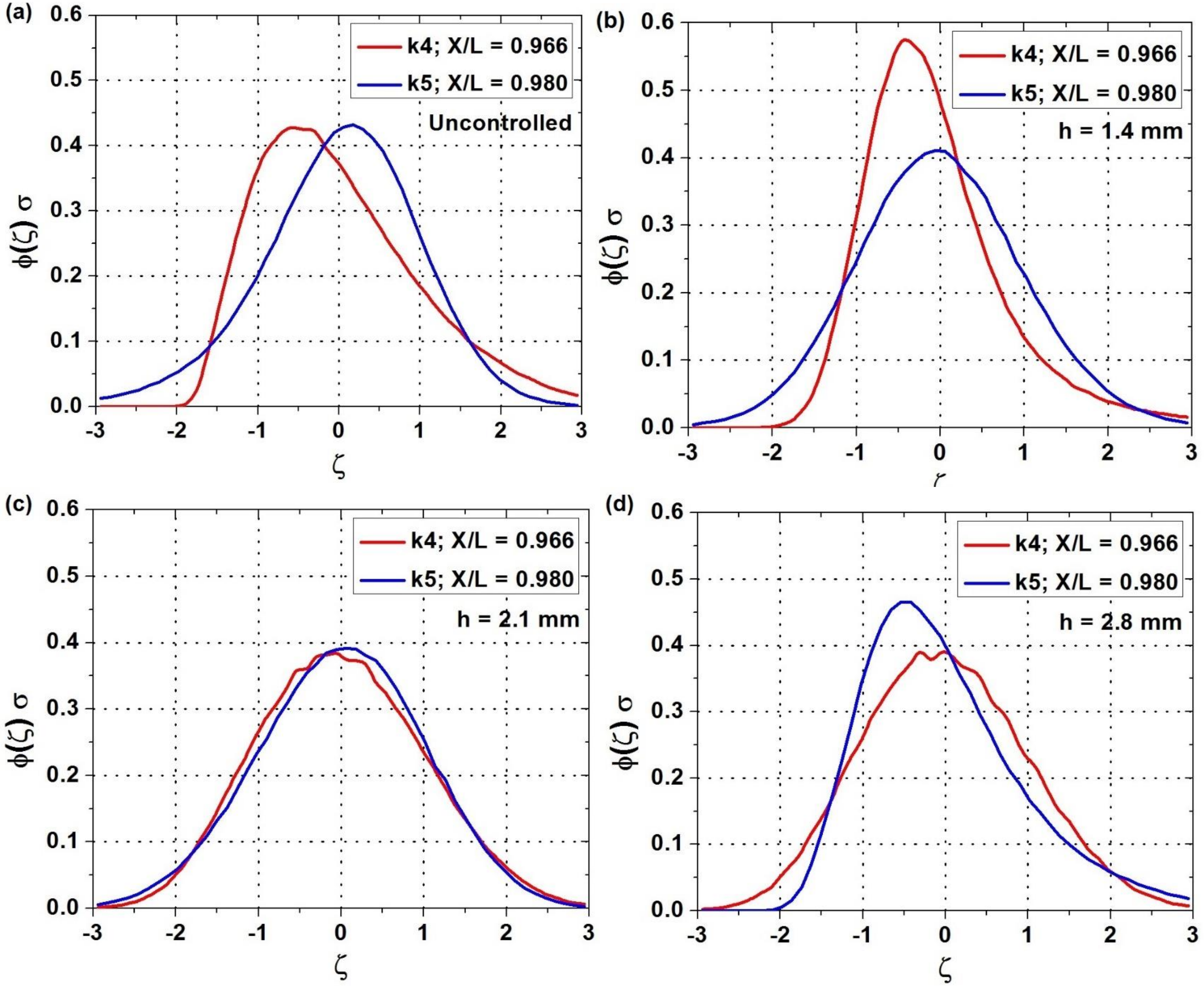

Intermittent characteristics of the separation shock

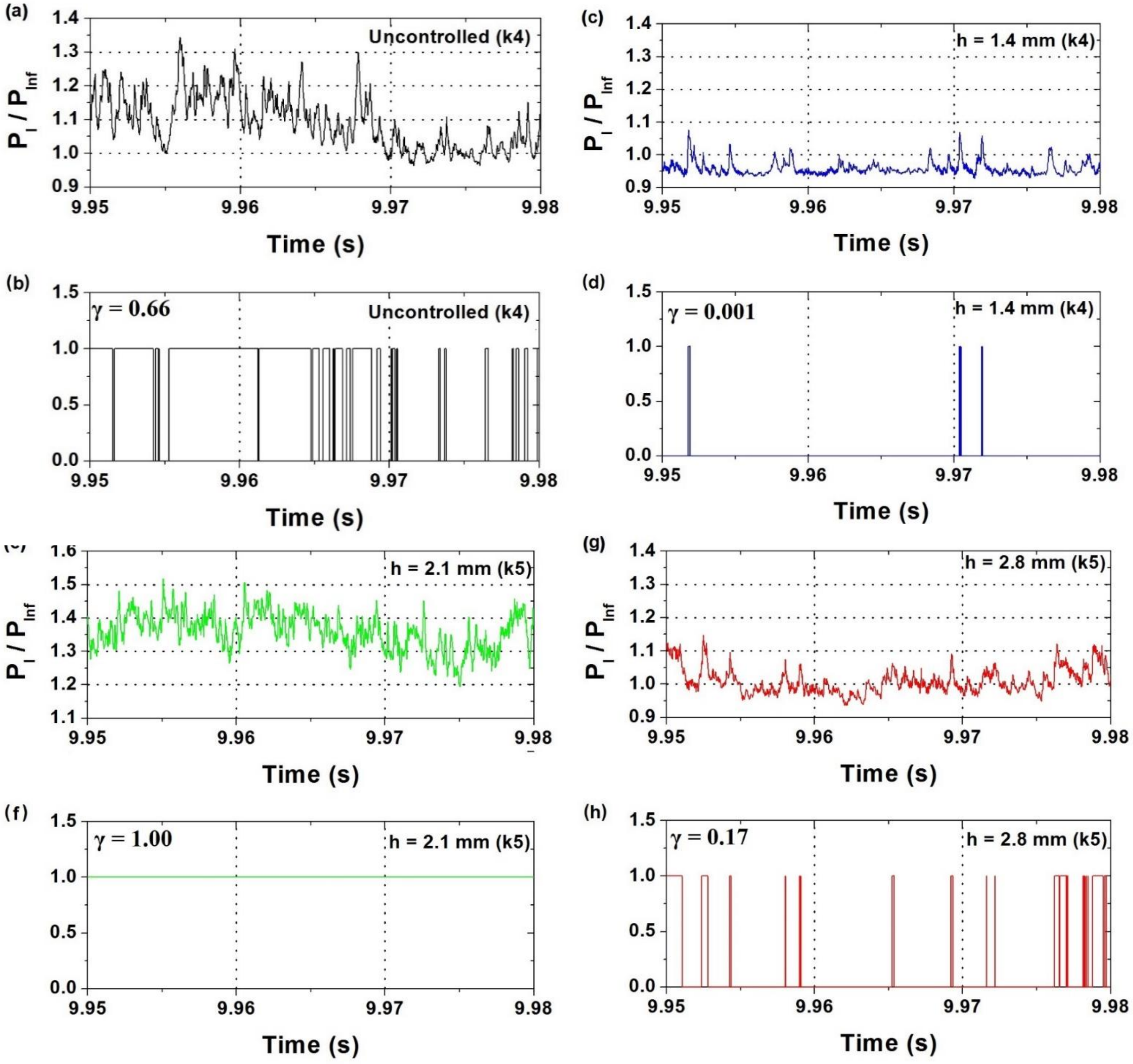

No meaningful variation in the separation shock's low-frequency characteristics, despite significant push-back of the intermittent region.

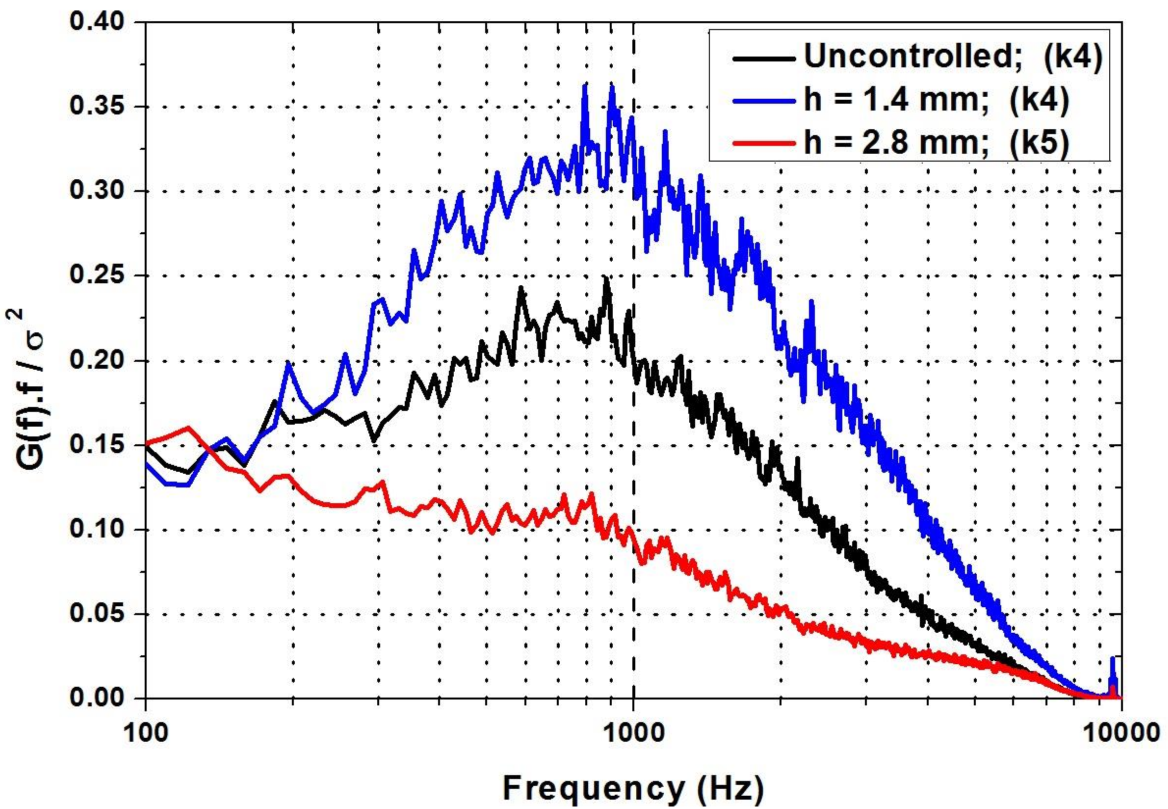

Surface pressure distribution near the MVGs

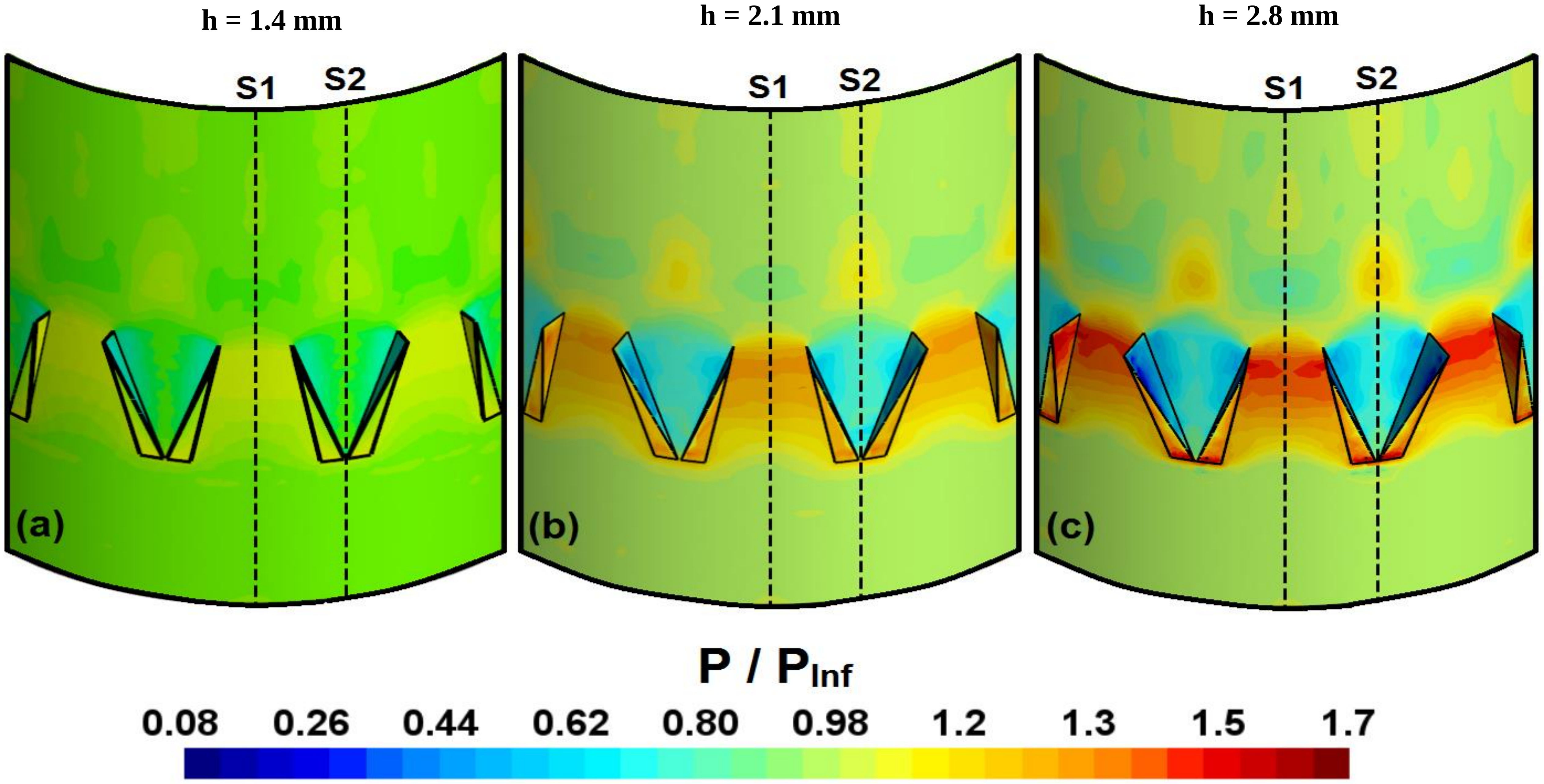

Streamwise vorticity at 20 mm upstream of the corner

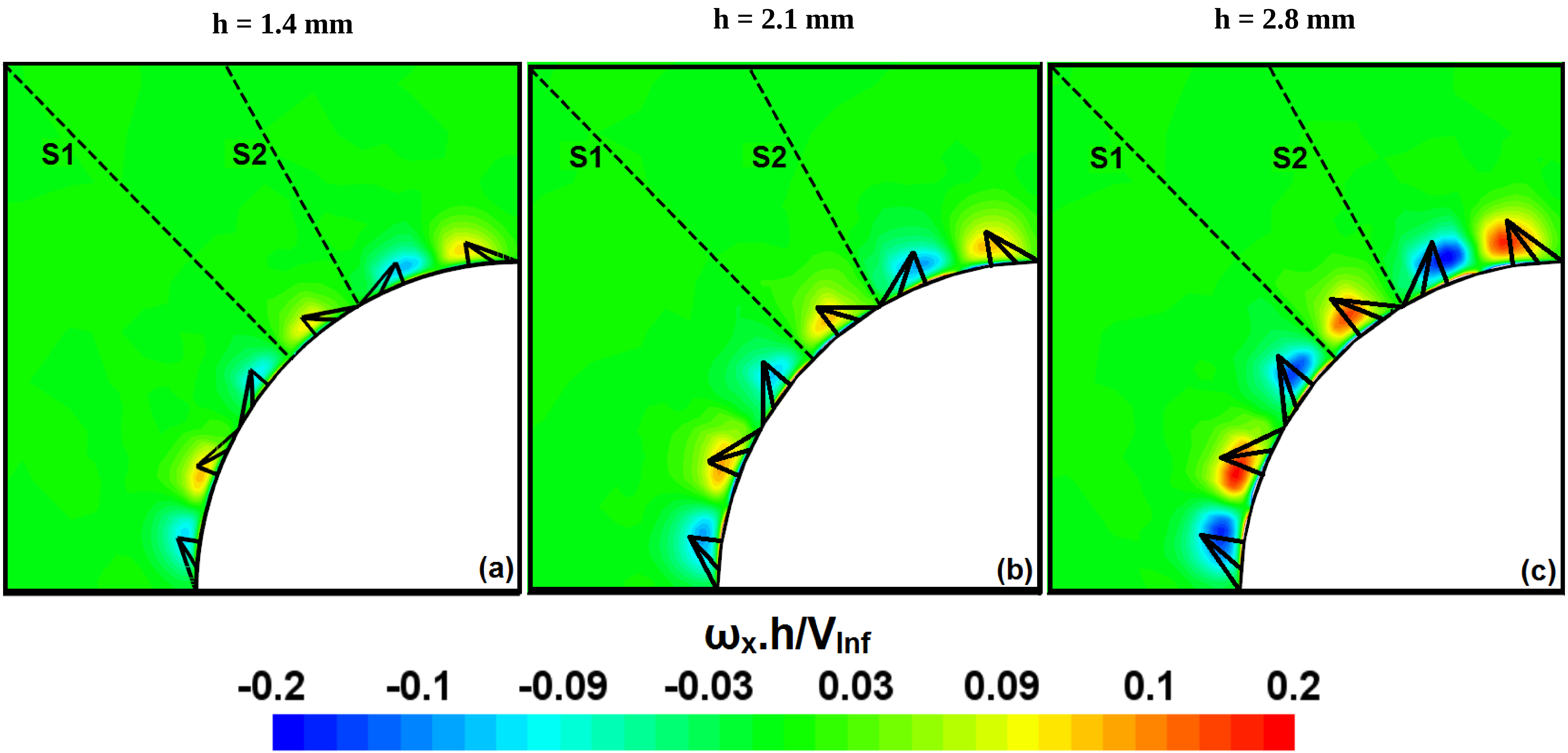

Relative velocity at 20 mm upstream of the corner

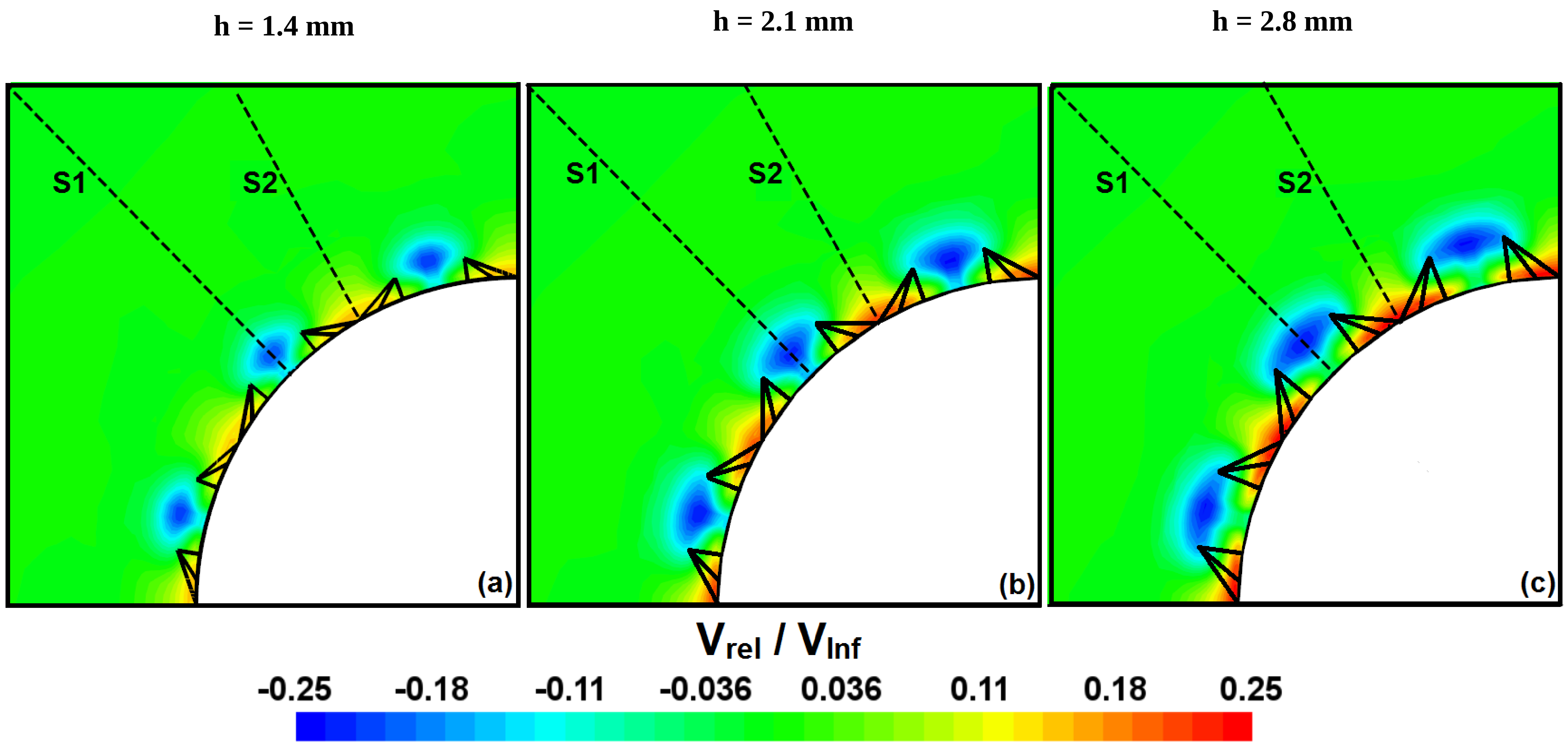

Effect of streamwise position – Ramped Vanes (h = 1.4 mm)

(a) Isometric view of a single RV device,

(b) Planform view showing the Kulite location with respect to the device centreline

(c) (c) Three streamwise positions of the RV array with respect to the compression corner

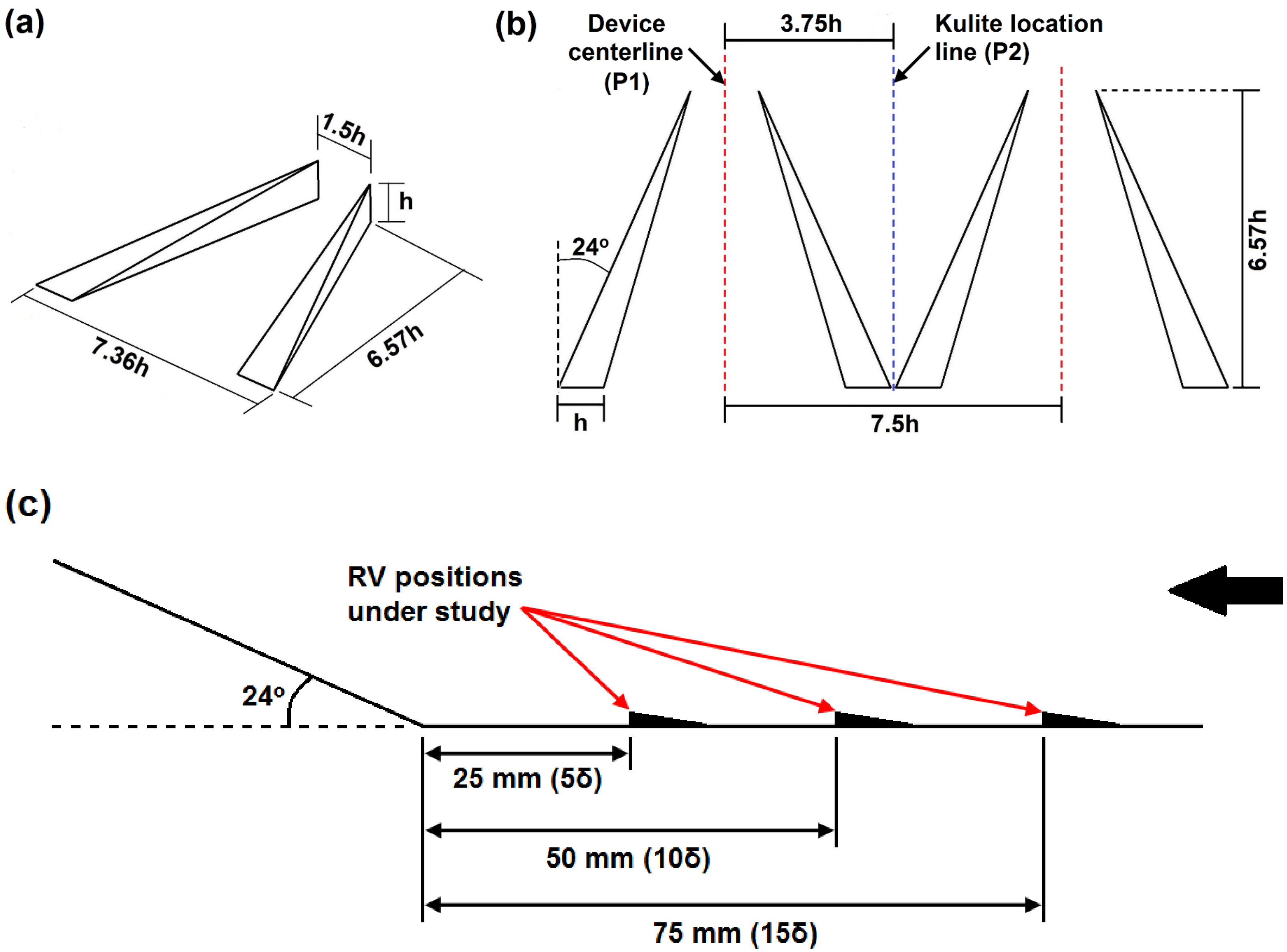

Surface pressure distributions

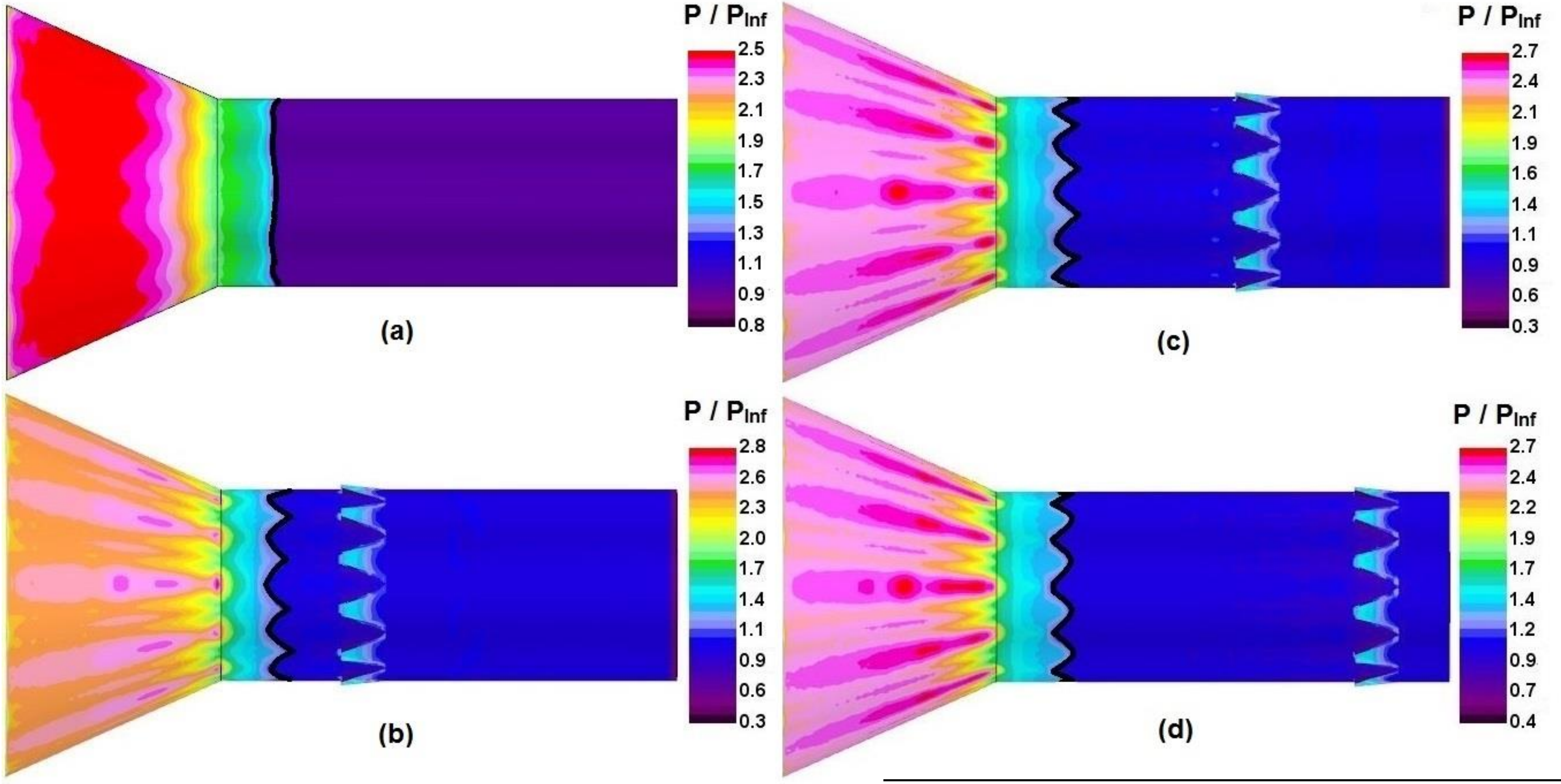

(a) Uncontrolled

(b) X_{RV} = -5δ

(c) X_{RV} = -10δ

(d) X_{RV} = -15δ

Configuration	(UI)	UI / UI_{UC}
UC (UI_{UC})	2.80 δ	1.00
X_{RV} = -5δ	2.74 δ	0.98
X_{RV} = -10δ	2.99 δ	1.07
X_{RV} = -15δ	3.15 δ	1.25

Surface streamline visualizations and critical points

- Spade shaped patterns widened along the azimuthal direction as the RV array was moved away from the interaction

- Narrowing of the attached flow pockets.

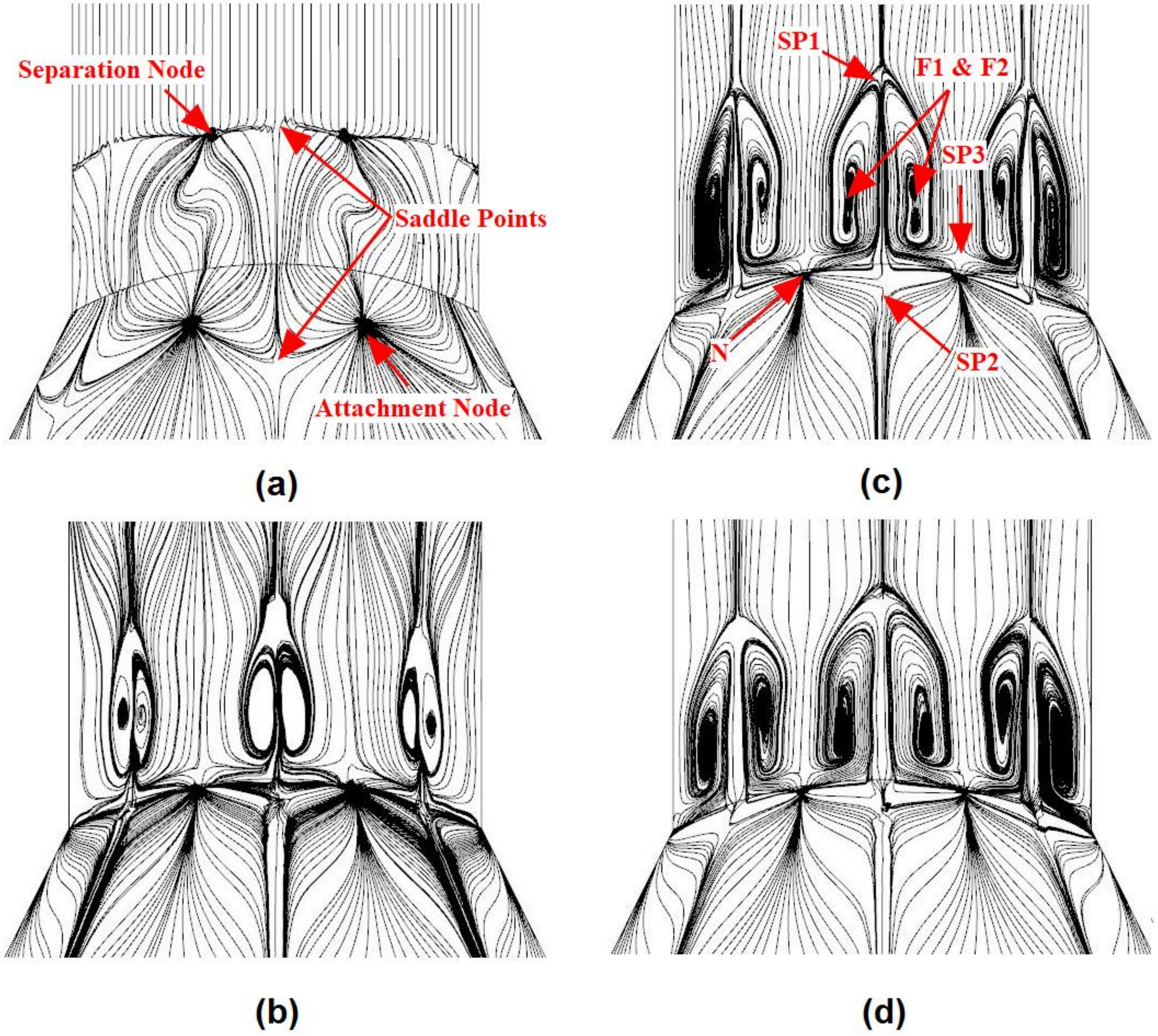

(a) Uncontrolled; (b) X_{RV} = -5δ; (c) X_{RV} = -10δ; (d) X_{RV} = -15δ

Conclusions

1. Among the different MVG shapes that were investigated, Ramped Vanes (RV) appeared to be the best suited for separation control, as they produced the strongest vortices and reduced vortex decay by preventing interaction between vortices originating from the same devices.

2. The streamwise vortices produced conspicuous alterations in the three-dimensional separated flow topology, which indicated that the separation region broke up into a series of tornado-like vortical structures.

3. Larger/taller devices were more successful in delaying the onset of separation throughout the circumference of the model. However, the device drag incurred and the possibility of having a strong local SBLI ahead of these devices should be taken into account.

4. The separation shock's oscillations were relatively broadband (0.55 kHz to 0.9 kHz) and the MVGs (except in one case) were unable to cause any meaningful favourable alterations in its temporal characteristics. More comprehensive investigations are required on the MVG's influence on shock oscillations.

Major outcomes

1. This is the first comprehensive work that investigates the control of SWBLI occurring over slender body vehicles such as rockets and missiles.

2. Successfully demonstrated a delay in the onset of flow separation using Micro Vortex Generators.

3. Although more thorough studies are required, there is preliminary evidence that these devices have the potential to push the shock oscillations away from structural resonant frequencies.

4. MVGs smaller than 50% of the local boundary layer thickness are unlikely to have a favourable impact.

THANK YOU